The *lhfpl5* ohnologs *lhfpl5a* and *lhfpl5b* are required for mechanotransduction in distinct populations of sensory hair cells in zebrafish.

Timothy Erickson[1, 2*], Itallia V. Pacentine[2], Alexandra Venuto[1], Rachel Clemens[2], and Teresa Nicolson[2, 3]

[1] Department of Biology, East Carolina University, Greenville, NC, USA.

[2] Vollum Institute and Oregon Hearing Research Center, OHSU, Portland, OR, USA.

[3] Current address: Otolaryngology-Head & Neck Surgery, Stanford School of Medicine, Stanford, CA, USA

*** Correspondence:**
Dr. Timothy Erickson, Department of Biology, East Carolina University, Greenville, NC, USA.
ericksonti17@ecu.edu

Keywords: hair cell, mechanotransduction, deafness, lateral line, zebrafish, LHFPL5, TMC1, PCDH15

Article type

Original Research

1 Abstract

Hair cells sense and transmit auditory, vestibular, and hydrodynamic information by converting mechanical stimuli into electrical signals. This process of mechano-electrical transduction (MET) requires a mechanically-gated channel localized in the apical stereocilia of hair cells. In mice, lipoma HMGIC fusion partner-like 5 (LHFPL5) acts as an auxiliary subunit of the MET channel whose primary role is to correctly localize PCDH15 and TMC1 to the mechanotransduction complex. Zebrafish have two *lhfpl5* genes (*lhfpl5a* and *lhfpl5b*), but their individual contributions to MET channel assembly and function have not been analyzed.

Here we show that the zebrafish *lhfpl5* genes are expressed in discrete populations of hair cells: *lhfpl5a* expression is restricted to auditory and vestibular hair cells in the inner ear, while *lhfpl5b* expression is specific to hair cells of the lateral line organ. Consequently, *lhfpl5a* mutants exhibit defects in auditory and vestibular function, while disruption of *lhfpl5b* affects hair cells only in the lateral line neuromasts. In contrast to previous reports in mice, localization of Tmc1 does not depend upon Lhfpl5 function in either the inner ear or lateral line organ. In both *lhfpl5a* and *lhfpl5b* mutants, GFP-tagged Tmc1 and Tmc2b proteins still localize to the stereocilia of hair cells. Using a stably integrated GFP-Lhfpl5a transgene, we show that the tip link cadherins Pcdh15a and Cdh23, along with the Myo7aa motor protein, are required for correct Lhfpl5a localization at the tips of stereocilia. Our work corroborates the evolutionarily conserved co-dependence between Lhfpl5 and Pcdh15, but also reveals novel requirements for Cdh23 and Myo7aa to correctly localize Lhfpl5a. In addition, our data suggest that targeting of Tmc1 and Tmc2b proteins to stereocilia in zebrafish hair cells occurs independently of Lhfpl5 proteins.

2 Introduction

The mechano-electrical transduction (MET) complex of sensory hair cells is an assembly of proteins and lipids that facilitate the conversion of auditory, vestibular and hydrodynamic stimuli into electrical signals. Our current understanding is that the proteins of the MET complex consist of the tip link proteins cadherin 23 (CDH23) and protocadherin 15 (PCDH15) at the upper and lower ends of the tip link respectively (Kazmierczak et al., 2007), the pore-forming subunits transmembrane channel-like proteins TMC1 and TMC2 (Kawashima et al., 2011; Pan et al., 2013, 2018), and the accessory subunits transmembrane inner ear (TMIE) and lipoma HMGIC fusion partner-like 5 (LHFPL5) (Cunningham and Müller, 2019; Xiong et al., 2012; Zhao et al., 2014). How these proteins are correctly localized to the sensory hair bundle and assemble into a functional complex is a fundamental question for understanding the molecular basis of how mechanotransduction occurs.

Recent studies have revealed extensive biochemical interactions between the MET complex proteins that are required for the function and / or stable integration of each component in the complex. In particular, LHFPL5 is a central player in MET complex formation, stability, and function. LHFPL5 (a.k.a. tetraspan membrane protein of the hair cell stereocilia / TMHS) is a four transmembrane domain protein from the superfamily of tetraspan junctional complex proteins. This superfamily includes junctional proteins like claudins and connexins, as well as ion channel auxiliary subunits such as transmembrane α-amino-3-hydroxy-5-methyl-4-isoxazole propionic acid receptor (AMPAR) regulatory proteins (TARPs) and the gamma subunits of voltage gated calcium channels. Pathogenic mutations in LHFPL5 are a cause of non-syndromic sensorineural hearing loss in humans (DFNB67), mice and zebrafish (Longo-Guess et al., 2005; Nicolson et al., 1998; Obholzer et al., 2012; Shabbir et al., 2006). LHFPL5 localizes to the tips of stereocilia (Li et al., 2019; Mahendrasingam et al., 2017; Xiong et al., 2012) where it directly interacts with other MET complex components. Co-immunoprecipitation experiments in heterologous cells suggests that LHFPL5 can directly interact with PCDH15 and TMIE (Xiong et al., 2012; Zhao et al., 2014). A structure of the PCDH15 - LHFPL5 complex has also been reported (Ge et al., 2018).

A precise role for LHFPL5 has yet to be defined. One current hypothesis is that LHFPL5 acts as an auxiliary subunit of the MET channel to stabilize the complex, similar to TARPs and the gamma subunits of voltage-gated calcium channels. In mouse cochlear hair cells, PCDH15 and LHFPL5 require each other for stable localization to the tips of stereocilia (Mahendrasingam et al., 2017; Xiong et al., 2012), consistent with their well-defined biochemical interaction. Interestingly, although experiments have failed to demonstrate a biochemical interaction between LHFPL5 and the TMCs, LHFPL5 is required for the localization of TMC1, but not TMC2, in the hair bundle of mouse cochlear hair cells (Beurg et al., 2015). The basis for the selective loss of TMC1 is not known. The partial loss of PCDH15 from the stereocilia explains the observed reduction in the number of tip links and the dysmorphic hair bundles in *Lhfpl5*$^{-/-}$ hair cells. In the absence of TMC1, a TMC2-dependent MET current still persists in mouse *Lhfpl5* mutants.

In zebrafish, Lhfpl5a plays a similar role in mechanotransduction as its mammalian counterparts. A mutation in zebrafish *lhfpl5a* was reported in a forward genetic screen for genes required for hearing and balance (Nicolson et al., 1998; Obholzer et al., 2012). The loss of Lhfpl5a disrupts the targeting of Pcdh15a to stereocilia and results in splayed hair bundles (Maeda et al., 2017). However, Lhfpl5a is not required to correctly localize Tmie and vice versa (Pacentine and Nicolson, 2019), in spite of their biochemical interaction in cultured cells (Xiong et al., 2012). Lhfpl5 still localizes to the tips of stereocilia in *Tmc1*/*Tmc2* double mutants (Beurg et al., 2015), as well as *transmembrane O-methyltransferase* (*tomt*) mouse and zebrafish mutants, which fail to traffic TMCs to the hair bundle

(Cunningham et al., 2017; Erickson et al., 2017). This phenotype suggests that Lhfpl5 localization does not require the TMCs. However, a number of questions regarding the functions of Lhfpl5 remain unanswered: 1) In zebrafish, what are the molecular requirements for targeting Lhfpl5a to the hair bundle? 2) Is the Lhfpl5-dependent targeting of Tmc1 to the hair bundle an evolutionarily-conserved aspect of their interaction? 3) *lhfpl5a* mutants have defects in auditory and vestibular behaviors, yet sensory hair cells of the lateral line are unaffected (Nicolson et al., 1998). What is the genetic basis for the persistence of lateral line function in *lhfpl5a* mutants?

In this work, we report that teleost fish have two *lhfpl5* genes, *lhfpl5a* and *lhfpl5b*. The zebrafish *lhfpl5* ohnologs are expressed in distinct populations of larval sensory hair cells: *lhfpl5a* in the auditory and vestibular system; *lhfpl5b* in the hair cells of the lateral line organ. This cis-regulatory divergence explains why lateral line hair cells are still mechanically-sensitive in *lhfpl5a* mutants. CRISPR-Cas 9 knockout of *lhfpl5b* alone silences the lateral line organ but has no effect on otic hair cell function. We also show that neither Lhfpl5a nor Lhfpl5b are required for Tmc localization in stereocilia. Additionally, we use a GFP-tagged Lhfpl5a to demonstrate that Myo7aa and the tip link proteins Cdh23 and Pcdh15a are required for proper Lhfpl5a localization in otic hair cell bundles. This study reveals the subfunctionalization of the zebrafish *lhfpl5* ohnologs through cis-regulatory divergence. Furthermore, our work complements previous results from murine cochlear hair cells by highlighting a conserved association between Lhfpl5 and Pcdh15, but also demonstrating novel requirements for Cdh23 and Myo7aa in localizing Lhfpl5a. Lastly, our work indicates that Lhfpl5-dependent localization of Tmc1 is not a universal feature of sensory hair cells and that Lhfpl5 proteins are required for mechanotransduction independently of a role in localizing the Tmc channel subunits to stereocilia.

3 Materials and Methods

3.1 Ethics statement

Animal research complied with guidelines stipulated by the Institutional Animal Care and Use Committees at Oregon Health and Science University (Portland, OR, USA) and East Carolina University (Greenville, NC, USA). Zebrafish (*Danio rerio*) were maintained and bred using standard procedures (Westerfield, 2000).

3.2 Mutant and transgenic fish lines

The following zebrafish mutant alleles were used for this study: *cdh23*^{nl9}, *cdh23*^{tj264}, *lhfpl5a*^{tm290}, *lhfpl5b*^{vo35}, *myo7aa*^{ty220}, *pcdh15a*^{psi7}, *pcdh15a*^{th263b} (Erickson et al., 2017; Ernest et al., 2000; Maeda et al., 2017; Nicolson et al., 1998; Obholzer et al., 2012). The transgenic lines used in this study were *Tg(-6myo6b:eGFP-lhfpl5a)*^{vo23Tg}, *Tg(-6myo6b:tmc1-emGFP)*^{vo27Tg}, *Tg(-6myo6b:tmc2b-emGFP)*^{vo28Tg} (Erickson et al., 2017), and *Tg(-6myo6b:eGFP-pA)*^{vo68Tg}. All experiments used larvae at 1–7 dpf, which are of indeterminate sex at this stage.

3.3 Genotyping

Standard genomic PCR followed by Sanger sequencing was used to identify *cdh23*^{tj264}, *cdh23*^{nl9}, *lhfpl5a*^{tm290d}, *pcdh15a*^{psi7}, and *pcdh15a*^{th263b} alleles. The *lhfpl5b*^{vo35} mutation disrupts a MluCI restriction site (AATT) and we are able to identify *lhfpl5b*^{vo35} hetero- and homozygotes based on the different sizes of MluCI-digested PCR products resolved on a 1.5% agarose gel. The following primers were used for genotyping:

124 *cdh23*^{nl9}: Fwd – CCACAGGAATTCTGGTGTCC, Rvs – GAAAGTGGGCGTCTCATCAT;

125 *cdh23*^{tj264}: Fwd – GGACGTCAGTGTTCATGGTG, Rvs – TTTTCTGACCGTGGCATTAAC;

126 *lhfpl5a*^{tm290d}: Fwd – GGACCATCATCTCCAGCAAAC, Rvs –
127 CACGAAACATATTTTCACTCACCAG;

128 *lhfpl5b*^{vo35}: Fwd – GCGTCATGTGGGCAGTTTTC, Rvs – TAGACACTAGCGGCGTTGC;

129 *myo7aa*^{ty220}: Fwd – TAGGTCCTCTTTAATGCATA, Rvs –
130 GTCTGTCTGTCTGTCTATCTGTCTCGCT;

131 *pcdh15a*^{psi7}: Fwd – TTGGCACCACTATCTTTACCG, Rvs – ACAGAAGGCACCTGGAAAAC;

132 *pcdh15a*^{th263b}: Fwd – AGGGACTAAGCCGAAGGAAG, Rvs –
133 CACTCATCTTCACAGCCATACAG.

134 **3.4 Phylogeny**

135 Lhfpl5 protein sequences retrieved from either NCBI or Ensembl (Supplemental Table 1).
136 Phylogenetic analysis was done on www.phylogeny.fr using T-Coffee (multiple sequence alignment),
137 GBlocks (alignment curation), PhyML (maximum likelihood tree construction with 100 replicates to
138 estimate bootstrap values), and TreeDyn (visualization) (Dereeper et al., 2008).

139 **3.5 mRNA *in situ* hybridization**

140 *lhfpl5a* and *lhfpl5b* probe templates were amplified from total RNA using the following primers:
141 *lhfpl5a* Fwd: AATATTGGTGCATAGACTCAAGGAGG; Rvs:
142 GACTCCAAAATGACCTTTTAACAAACGC. *lhfpl5b* Fwd:
143 TGAAGATCAGCTACGATATAACCGG; Rvs: ACTGTGATTGGTGTATTTCCAGC. The inserts
144 were cloned into the pCR4 vector for use in probe synthesis. mRNA *in situ* probe synthesis and
145 hybridization was performed essentially as previously described (Erickson et al., 2010; Thisse and
146 Thisse, 2008). Stained specimens were mounted on a depression slide in 1.2 % low-melting point
147 agarose and imaged on a Leica DMLB microscope fitted with a Zeiss AxioCam MRc 5 camera using
148 Zeiss AxioVision acquisition software (Version 4.5).

149 **3.6 Immunofluorescent staining, FM dye labeling, and fluorescence microscopy**

150 Anti-Pcdh15a immunostaining and FM dye labeling of inner ear and lateral line hair cells were
151 performed as previously described (Erickson et al., 2017). All fluorescent imaging was done on Zeiss
152 LSM 700 or LSM 800 laser scanning confocal microscopes. Z-stacks were analyzed using ImageJ
153 (Schneider et al., 2012). All related control and experimental images were adjusted equally for
154 brightness and contrast in Adobe Photoshop CC.

155 **3.7 CRISPR-Cas9 knockout of *lhfpl5b***

156 An sgRNA targeting the *lhfpl5b* sequence 5'- CAACCCAATCACCTCGGAAT-3' was synthesized
157 essentially as described (Gagnon et al., 2014). For microinjection, 1 ug of sgRNA was mixed with 1
158 ug of Cas9 protein and warmed to 37ºC for 5 minutes to promote the formation of the Cas9-sgRNA
159 complex. Approximately 2 nl of this solution was injected into wild type embryos at the single-cell
160 stage. Efficacy of cutting was determined in two ways: 1) Single larvae genotyping - Amplification of

161 the target genomic region by PCR and running the products on 2.5% agarose gels to assay for disruption
162 of a homogenous amplicon. 2) Assaying for disruption of the mechanotransduction channel in lateral
163 line hair cells by FM 1-43 dye uptake. Larvae displaying a non-wild type pattern of FM 1-43 dye uptake
164 were raised to adulthood. Progeny from in-crosses of F0 adults were exposed to FM 1-43 dye to identify
165 founders. By outcrossing founder adults, we established a line of fish carrying a 5 base pair deletion in
166 the *lhfpl5b* coding region that causes a S77FfsX48 mutation (*lhfpl5b*^{vo35}). This mutation disrupts the
167 protein in the first extracellular loop and deletes the final three of four transmembrane helices in
168 Lhfpl5b.

169 **3.8 Acoustic startle response**

170 Quantification of the larval acoustic startle response was performed using the Zebrabox monitoring
171 system (ViewPoint Life Sciences, Montreal, Canada) as previously described (Maeda et al., 2017) with
172 the following modifications. Each trial included six larvae which were subjected to two or three trials
173 of 6 acoustic stimuli. For each individual larva, the trial with best AEBR performance was used for
174 quantification. Positive responses where spontaneous movement occurred in the second prior to the
175 stimulus were excluded from analysis. Trials where spontaneous movement occurred for more than 6
176 of the 12 stimuli were also excluded from analysis.

177 **3.9 Microphonics**

178 We performed the microphonic measurements as previously described (Pacentine and Nicolson, 2019).
179 In brief, we anesthetized 3 dpf larvae in extracellular solution (140mM NaCl, 2mM KCl, 2mM $CaCl_2$,
180 1mM $MgCl_2$, and 10mM 4-(2-hydroxyethyl)-1-piperazineethanesulfonic acid (HEPES); pH 7.4)
181 containing 0.02% 3-amino benzoic acid ethylester (MESAB; Western Chemical). We pinned the larvae
182 with two glass fibers straddling the yolk and a third perpendicular fiber to prevent sliding. For pipettes,
183 we used borosilicate glass with filament, O.D.: 1.5 mm, O.D.: 0.86 mm, 10 cm length (Sutter, item #
184 BF150-86-10, fire polished). Using a Sutter Puller (model P-97), we created recording pipettes with a
185 long shank with a resistance of 10-20MΩ, after which we beveled the edges to a resistance of 4-5 MΩ
186 using a Sutter Beveler with impedance meter (model BV-10C). For the glass probe delivering the piezo
187 stimulus, we pulled a long shank pipette and fire polished to a closed bulb. To completely ground the
188 piezo actuator, we had to shield the apparatus with tin foil. To maintain consistent delivery of stimulus,
189 we always pressed the probe to the front of the head behind the lower eye, level with the otoliths in the
190 ear of interest. We also maintained a consistent entry point dorsal to the anterior crista and lateral to
191 the posterior crista. During delivery of stimulus, the piezo probe made light contact with the head. We
192 drove the piezo with a High Power Amplifier (piezosystem jena, System ENT/ENV, serial # E18605),
193 and recorded responses in current clamp mode with a patch-clamp amplifier (HEKA, EPC 10 usb
194 double, serial # 550089). Voltage responses were amplified 1000x and filtered between 0.1-3000 Hz
195 by the Brownlee Precision Instrumentation Amplifier (Model 440). We used a 200 Hz sine wave
196 stimulus at 10 V and recorded at 20 kHz, collecting 200 traces per experiment. Each stimulus was of
197 40 ms duration, with 20 ms pre- and post-stimulus periods. The piezo signal was low-pass filtered at
198 500Hz using the Low-Pass Bessel Filter 8 Pole (Warner Instruments). In Igor Pro, we averaged each
199 set of 200 traces to generate one wave response per larva. To quantify hair cell activity, we calculated
200 the amplitude from base-to-peak of the first peak. Larvae were genotyped as described above.

201 **3.10 Hair cell counts**

202 *lhfpl5b*$^{vo35/+}$ fish were crossed with *Tg(myo6b:eGFP-pA)*^{vo68Tg}*; lhfpl5b*$^{vo35/+}$ fish to produce wild type
203 and *lhfpl5b*^{vo35} siblings expressing green fluorescent protein in hair cells. Wild type and mutant larvae
204 were genotyped by FM 4-64 labeling (n = 5 each) and fixed in 4% paraformaldehyde at 5 dpf. Specimen

were mounted in low melting point agarose and imaged on a Zeiss LSM 800 confocal. On each larva, three neuromasts were imaged; L1, MI1, and O2. From these images, the individual hair cells were counted for each neuromast on each fish, for a total of 15 neuromasts in both wild type and *lhfpl5b*^{vo35} zebrafish.

3.11 Statistics

Statistical analyses were done using either the R stats package in RStudio (R Core Team, 2019; RStudio Team, 2018) or SPSS v25. P-values of less than 0.05 were considered to be statistically significant. Plots were made using either GraphPad Prism v.6.0h or ggplot2 (Wickham, 2016).

3.12 Data availability

The raw data supporting the conclusions of this manuscript will be made available by the corresponding author, without undue reservation, to any qualified researcher.

4 Results

4.1 Teleost fish have ohnologous *lhfpl5* genes.

Genes that have been duplicated as a result of a whole genome duplication (WGD) event are known as *ohnologs* (Ohno, 1970; Wolfe, 2000). Due to the teleost-specific WGD, it is not uncommon to find ohnologous genes in teleost fish where other vertebrate classes possess a single gene. The *Danio rerio* (zebrafish) genome contains two *lhfpl5* genes: *lhfpl5a* (ENSDARG00000045023) and *lhfpl5b* (ENSDARG00000056458). To determine if *lhfpl5* duplication is general to the teleost lineage, we queried either GenBank or Ensembl databases to collect Lhfpl5 protein sequences for humans, mice, chick, frogs, and representative sequences from 14 phylogenetic orders of ray-finned fish (Actinopterygii), including 13 orders from the Teleostei infraclass and one from the Holostei infraclass (Supplemental Table 1). The latter (Spotted gar, *Lepisosteus oculatus*) is commonly used to infer the consequences of the teleost WGD, since the Holostei and Teleostei infraclasses diverged before the teleost WGD (Braasch et al., 2016). Phylogenetic analysis of the Lhfpl5 protein sequences supports the idea that duplicate *lhfpl5* genes originated from the teleost WGD event (Figure 1A). In all 13 teleost orders surveyed, there are two *lhfpl5* genes whose protein products cluster with either the *lhfpl5a* or *lhfpl5b* ohnolog groups. Based on available genomic data, there is no evidence that spotted gar fish have duplicated *lhfpl5* genes. Nor is there evidence that the Salmonid-specific WGD (Allendorf and Thorgaard, 1984) lead to further expansion of the *lhfpl5* family. These analyses suggest that the ancestral *lhfpl5* gene was duplicated in the teleost WGD and that the *lhfpl5* ohnologs were retained in all teleost species examined here.

Alignment of the zebrafish Lhfpl5a and Lhfpl5b proteins with those from human, mouse and chicken reveals that both zebrafish ohnologs retain the same protein structure (Figure 1B). Zebrafish Lhfpl5a and Lhfpl5b are 76% identical and 86% similar to one another (Needleman-Wunsch alignment). Compared to human LHFPL5, Lhfpl5a and Lhfpl5b are 70 / 65 % identical and 86 / 81 % similar respectively. The ENU-generated mutation in *lhfpl5a* (*tm290d*) (Obholzer et al., 2012) is indicated by the red triangle (K80X). To investigate the function of *lhfpl5b*, we generated a Cas9-induced lesion in the *lhfpl5b* gene in a similar location as the *tm290d* mutation. We recovered a line with a 5 base pair deletion leading to a frameshift mutation (*lhfpl5b*^{vo35}, red square; S77FfsX48).

4.2 *lhfpl5a* and *lhfpl5b* are expressed in distinct populations of sensory hair cells.

To characterize the spatial and temporal patterns of *lhfpl5a/b* gene expression, we performed whole mount mRNA *in situ* hybridization on zebrafish larvae at 1, 2, and 5-days post-fertilization (dpf) (Figure 2). After one day of development, there are nascent hair cells of the presumptive anterior and posterior maculae in the developing ear, but no lateral line hair cells at this stage. We detect *lhfpl5a* expression in the presumptive anterior and posterior maculae at 1 dpf (Figure 2A). No signal for *lhfpl5b* was observed at this time point (Figure 2B). At 2 dpf, we observe a clear distinction in the expression patterns of the *lhfpl5a* and *lhfpl5b* genes (Figure 2C, D). *lhfpl5a* continues to be expressed in the ear, but expression is not observed in the newly deposited neuromasts. Conversely, we detect *lhfpl5b* expression exclusively in the neuromasts at this stage. This divergence in *lhfpl5* ohnolog expression continues at 5 dpf, with *lhfpl5a* found exclusively in the sensory patches of the ear and *lhfpl5b* restricted to lateral lien hair cells (Figure 2E-J). Taken together, the distinct mRNA expression patterns of these ohnologs suggest that both *lhfpl5a* and *lhfpl5b* have been retained since the teleost whole genome duplication because of cis-regulatory divergence.

4.3 *lhfpl5a* mediates mechanosensitivity of otic hair cells.

lhfpl5a^{tm290d} (*astronaut / asn*) mutants were initially characterized by balance defects, an absence of the acoustic startle reflex, and a lack of brainstem Ca^{2+} signals after acoustic startle. However, neuromast microphonic potentials were normal (Nicolson et al., 1998). In light of our *in situ* hybridization data (Figure 2), these results suggest that *lhfpl5a* is required for auditory and vestibular hair cell function only. To test this possibility, we performed several functional assays measuring the activity of hair cells in the otic capsule. First, we tested macular hair cell activity (Lu and DeSmidt, 2013; Yao et al., 2016) by recording extracellular microphonic potentials from the inner ears of *lhfpl5a*^{tm290d} mutants, along with wild type and *lhfpl5b*^{vo35} larvae at 3 dpf. We then measured baseline-to-peak amplitude of the first peak to quantify activity. (Figure 3A). Consistent with the initial findings, we did not detect robust microphonic potentials from the inner ear of *lhfpl5a*^{tm290d} mutants. We measured an average first peak microphonic of 53.1 µV from *lhfpl5a*^{tm290d} mutants ($n = 7$), which was significantly less than the 296.2 µV average value of their WT siblings ($n = 4$) ($p = 0.01$, Welch's t-test). For the *lhfpl5b*^{vo35} mutants ($n = 6$), we measured an average first peak microphonic potential of 280.9 µV (205.3 µV excluding the outlier). These values were not significantly different from their WT siblings (average 243.8 µV; $p = 0.7$, $p = 0.5$ without outlier), but were significantly greater than the *lhfpl5a*^{tm290d} mutants ($p = 0.036$, $p = 0.01$ without outlier). Thus, *lhfpl5a*^{tm290d} mutants exhibit defects in inner ear function, while the *lhfpl5b*^{vo35} mutation has no effect on these hair cells. To further confirm the lack of function in *lhfpl5a*^{tm290d} mutants, we performed an acoustic startle test on larvae at 6 dpf (Figure 3B). Results confirm that *lhfpl5a*^{tm290d} mutants are profoundly deaf, displaying little to no response to acoustic stimuli ($p < 0.001$ compared to all other genotypes). Finally, we tested the basal MET channel activity of hair cells of the semi-circular canals by injecting FM 4-64 into the otic capsule and imaging the lateral cristae sensory patch. WT hair cells readily labeled with FM 4-64 whereas *lhfpl5a*^{tm290d} mutant cells showed no sign of dye internalization (Figure 3C-D). These three tests confirmed that all sensory patches in the otic capsule are inactive in *lhfpl5a*^{tm290d} mutants.

A *GFP-lhfpl5a* transgenic line of zebrafish - *Tg(myo6b:eGFP-lhfpl5a)*^{vo23Tg} - has been reported previously (Erickson et al., 2017). GFP-Lhfpl5a is present at the tips of stereocilia, similar to the localization observed for mouse LHFPL5 (Mahendrasingam et al., 2017; Xiong et al., 2012). To demonstrate that the GFP-Lhfpl5a protein is functional, we assayed for the recovery of the acoustic startle reflex and MET channel activity in homozygous *lhfpl5a*^{tm290d} mutants expressing the transgene. The startle reflex of *lhfpl5a*^{tm290d} mutants expressing GFP-Lhfpl5a were statistically indistinguishable

292 from non-transgenic and transgenic WT siblings (p = 0.48 and 0.26 respectively) (Figure 3B).
293 Likewise, FM 4-64 dye-uptake in the lateral cristae was restored to *lhfpl5a*^{tm290d} mutants expressing
294 GFP-Lhfpl5a (Figure 3E-F'). From these results we conclude that the hair bundle-localized GFP-
295 Lhfpl5a protein is functional and can rescue the behavioral and MET channel defects in *lhfpl5a*^{tm290d}
296 mutants.

297 **4.4 *lhfpl5b* mediates mechanosensitivity of lateral line hair cells.**

298 The divergent expression patterns of the *lhfpl5* ohnologs suggests that *lhfpl5b* alone may be mediating
299 mechanosensitivity of lateral line hair cells. To test this, we compared basal MET channel activity in
300 neuromast hair cells of WT, *lhfpl5a*^{tm290d} and *lhfpl5b*^{vo35} larvae using an FM 1-43 dye uptake assay
301 (Figure 4A-C). Strikingly, lateral line hair cells in *lhfpl5b*^{vo35} mutants do not label with FM 1-43 while
302 there is no obvious difference in the intensity of FM 1-43 labeling of hair cells between WT and
303 *lhfpl5a*^{tm290d} mutants (Figure 4A-C). We quantified this loss of lateral line function by measuring the
304 average FM 1-43 fluorescence intensity per hair cell in each imaged neuromast of *lhfpl5b*^{vo35} mutants
305 and wild type siblings at 2 dpf (Figure 4D, E, H) and 5 dpf (Figure 4F-H). *lhfpl5b*^{vo35} mutants exhibit
306 a statistically significant decrease in FM 1-43 uptake at both 2 dpf and 5 dpf (Welch's *t*-test, $p < 0.001$
307 both time points). While there is negligible FM dye labeling in the vast majority of *lhfpl5b*^{vo35} mutant
308 neuromasts, we occasionally observe labeling in some hair cells, most reproducibly in the SO3
309 neuromast. Occasional labeling persists in *lhfpl5a* / *lhfpl5b* double mutants, indicating that *lhfpl5a* is
310 not partially compensating for the loss of *lhfpl5b* (Supplemental Figure 1A-D). In addition to a lack of
311 basal MET channel activity in *lhfpl5b*^{vo35} mutant neuromasts, we also observe a statistically significant
312 decrease in the number of hair cells (Figure 4I, n = 5 individuals per genotype, 3 NM each, Welch's *t*-
313 test, $p < 0.05$ each NM type). This decrease is similar to what has been observed in other zebrafish
314 mechanotransduction mutants such as *myo7aa (mariner)*, *pcdh15a (orbiter)*, and *tomt (mercury)*
315 (Erickson et al., 2017; Seiler et al., 2005). The loss of MET channel activity in *lhfpl5b*^{vo35} neuromasts
316 is rescued by expression of the *GFP-lhfpl5a* transgene (Figure 4J, K; n = 7/7 mutant individuals). This
317 result indicates that Lhfpl5a and Lhfpl5b are functionally interchangeable in this context.

318 **4.5 *lhfpl5* is not required for Tmc localization to the hair bundle in zebrafish hair cells.**

319 Previous studies have demonstrated that loss of LHFPL5 leads to a ~90% reduction in the peak
320 amplitude of the transduction current in mouse cochlear outer hair cells (Xiong et al., 2012). Single
321 channel recordings from *Lhfpl5* mutants revealed that the remaining transduction current in *Lhfpl5*
322 mutants was mediated by TMC2 (Beurg et al., 2015). Using antibody staining to detect endogenous
323 TMC1, it was shown that TMC1 was absent from the bundle of *Lhfpl5* mouse mutants. However,
324 injectoporated Myc-TMC2 was still able to localize to the hair bundle, supporting the idea that LHFPL5
325 is required for the targeting of TMC1, but not TMC2. The localization of exogenously-expressed
326 TMC1 in *Lhfpl5* mutants was not reported.

327 To determine if the Tmcs require Lhfpl5a for localization to the hair bundle of zebrafish hair cells, we
328 bred stable transgenic lines expressing GFP-tagged versions of Tmc1 (*vo27Tg*) and Tmc2b (*vo28Tg*)
329 (Erickson et al., 2017) into the *lhfpl5a*^{tm290d} mutant background and imaged Tmc localization in the
330 lateral cristae of the ear. In contrast to what was observed in mouse cochlear hair cells, both Tmc1-
331 GFP and Tmc2b-GFP are still targeted to the hair bundle in *lhfpl5a*^{tm290d} mutants (n = 11/11 and 9/9
332 individuals respectively; Figure 5A-D'). We also observe Tmc2b-GFP localization in the neuromast
333 hair bundles of *lhfpl5b*^{vo35} mutants (n = 7/7 individuals; Figure 5E-F'). Additionally, we do not observe
334 any rescue of hair cell function in *lhfpl5b* mutants expressing the Tmc2b-GFP protein (Supplemental
335 Figure 2A-C). As such, these results suggest that GFP-tagged Tmc1 and Tmc2b do not require Lhfpl5
336 for hair bundle localization in zebrafish hair cells.

4.6 GFP-Lhfpl5a localization in stereocilia requires Pcdh15a, Cdh23, and Myo7aa.

Previous work has shown that PCDH15 and LHFPL5 are mutually dependent on one another to correctly localize to the site of mechanotransduction in mouse cochlear hair cells (Mahendrasingam et al., 2017; Xiong et al., 2012). Likewise in zebrafish, Lhfpl5a is required for proper Pcdh15a localization in the hair bundle, as determined Pcdh15a immunostaining and the expression of a Pcdh15a-GFP transgene in *lhfpl5a*^{tm290d} mutants (Maeda et al., 2017). Using the previously characterized antibody against Pcdh15a, we observe the highest level of Pcdh15a staining at the apical part of the hair bundle, with less intense punctate staining throughout the stereocilia in 3 dpf wild type larvae (Figure 6A). *lhfpl5a*^{tm290d} mutants exhibit splayed hair bundles, with low levels of Pcdh15a staining restricted to the tip of each stereocilium (n = 5/5 individuals; Figure 6B), confirming our previous report.

To determine if Lhfpl5a also depends on Pcdh15a for its localization, we imaged GFP-Lhfpl5 in the lateral cristae of *pcdh15a*^{psi7} homozygous mutants. In wild type larvae, GFP-Lhfpl5a is distributed throughout the hair bundle at the tips of stereocilia (yellow arrow heads), with a higher intensity of GFP evident in the tallest rows, possibly at the sites of kinociliary links (Figure 6C, C', arrow). In *pcdh15a*^{psi7} mutants, GFP-Lhfpl5a is absent from the hair bundle except for the tallest rows of stereocilia adjacent to the kinocilium (n = 4 individuals; Figure 6D, D', arrow). We observed similar results using the *pcdh15a*^{th263b} allele (n = 6/6 individuals; Supplemental Figure 3A, B). These results indicate that GFP-Lhfpl5a requires Pcdh15a for stable targeting to the shorter stereocilia, but Pcdh15a is not required for retaining GFP-Lhfpl5a in the tallest rows of stereocilia adjacent to the kinocilium.

The observation that some GFP-Lhfpl5a signal remains in the tallest stereocilia of *pcdh15a* mutants suggests that additional proteins are involved in targeting Lhfpl5a to these sites in zebrafish vestibular hair cells. Previous research has shown that mouse CDH23 still localizes to tips of stereocilia in PCDH15-deficient mice (Boëda et al., 2002; Senften et al., 2006) and that CDH23 is a component of kinociliary links (Goodyear et al., 2010; Siemens et al., 2004). Based on these reports, we tested whether Cdh23 was required for GFP-Lhfpl5a localization. In *cdh23*^{nl9} mutants, GFP-Lhfpl5 is sparsely distributed throughout the length of the kinocilium (n = 4/4 individuals, Figure 6E, E'). We also observe a redistribution of GFP-Lhfpl5a into the kinocilium using the *cdh23*^{tj264} allele (n = 4/4 individuals; Supplemental Figure 3C). In both *cdh23* alleles, we see occasional GFP signal in the stereocilia as well, though this localization is not as robust. Interestingly, these results contrast with those from mouse cochlear hair cells which showed that Lhfpl5 does not require Cdh23 for bundle localization (Zhao et al., 2014). The same study also could not detect any biochemical interaction between LHFPL5 and proteins of the upper tip link density including CDH23, USH1C / Harmonin, or USH1G / Sans. Together, our data indicate an unexpected role for Cdh23 in the localization of GFP-Lhfpl5a to the region of kinocilial links in zebrafish vestibular hair cells.

Myosin 7A (MYO7A) is an actin-based motor protein required for the localization of many proteins of the hair bundle, including PCDH15 and USH1C / Harmonin, along with several proteins of the Usher type 2 complex (Boëda et al., 2002; Lefevre et al., 2008; Maeda et al., 2017; Morgan et al., 2016; Senften et al., 2006; Zou et al., 2017). Results in both mice and zebrafish suggest that MYO7A is not required for CDH23 bundle localization (Blanco-Sanchez et al., 2014; Senften et al., 2006). However, its role in Lhfpl5 localization has not been examined. In *myo7aa*^{ty220} (*mariner*) mutant hair cells, GFP-Lhfpl5a localization in hair bundle is severely disrupted (n = 5/5 individuals; Figure 6 F, F'). We observe GFP signal near the base of hair bundles and occasionally in stereocilia (yellow arrowheads), but do not see robust Lhfpl5a localization in the presumptive kinocilial links nor to the kinocilium

itself. Taken together, our results using the GFP-Lhfpl5a transgene suggest that Pcdh15a, Cdh23, and Myo7aa all play distinct roles in Lhfpl5 localization in the bundle of zebrafish vestibular hair cells.

5 Discussion

In this study, we demonstrate the following points: 1) The ancestral *lhfpl5* gene was likely duplicated as a result of the teleost whole genome duplication, leading to the *lhfpl5a* and *lhfpl5b* ohnologs described in this paper. 2) In zebrafish, there has been subfunctionalization of these genes as a result of cis-regulatory divergence in their expression patterns. As determined by mRNA *in situ* hybridization, *lhfpl5a* is expressed only in auditory and vestibular hair cells of the ear while *lhfpl5b* is expressed solely in hair cells of the lateral line organ. Consistent with their expression patterns, we show that each ohnolog mediates mechanotransduction in the corresponding populations of sensory hair cells in zebrafish. 3) Targeting of GFP-tagged Tmcs to the hair bundle is independent of Lhfpl5a function. 4) Proper targeting of GFP-tagged Lhfpl5a to the hair bundle requires the tip link protein Pcdh15a, but as in mice, Lhfpl5a can localize to regions of the hair bundle independently of Pcdh15 function. Additionally, we demonstrate novel requirements for Cdh23 and the Myo7aa motor protein in Lhfpl5 localization.

5.1 Duplicated zebrafish genes in hair cell function.

With regards to genes involved in hair cell function, the zebrafish duplicates of *calcium channel, voltage-dependent, L type, alpha 1D* (*cacna1d* / *cav1.3*), *C-terminal binding protein 2* (*ctbp2* / *ribeye*), *myosin 6* (*myo6*), *otoferlin* (*otof*), *pcdh15*, and *tmc2* have been analyzed genetically. In the cases of *cacna1db*, *pcdh15b* and *myo6a*, these ohnologs are no longer functional in hair cells (Seiler et al., 2004, 2005; Sidi et al., 2004). For the *ctbp2*, *otoferlin*, and *tmc2* duplicates, both genes are required in at least partially overlapping populations of hair cells (Chou et al., 2017; Lv et al., 2016; Maeda et al., 2014; Sheets et al., 2011). In contrast, our results for the *lhfpl5* ohnologs suggest that each gene is expressed and functionally required in distinct, non-overlapping hair cell lineages. To our knowledge, this is the first description of duplicated genes whose expression patterns have cleanly partitioned between inner ear and lateral line hair cells.

5.2 Subfunctionalization of zebrafish *lhfpl5* ohnologs through cis-regulatory divergence.

Using Lhfpl5 protein sequence data gathered from genomic databases, we constructed a phylogenetic tree suggesting that the ancestral *lhfpl5* gene was duplicated during the teleost WGD event and that both genes have been retained throughout the teleost lineage (Figure 1). A recent detailed analysis of teleost genomes supports our conclusion that *lhfpl5a* and *lhfpl5b* are ohnologs (Singh and Isambert, 2019). Cis-regulatory divergence is a mechanism that selects for the retention of duplicated genes - both copies are still required because the expression pattern of the ancestral gene has been partitioned between the duplicates (Force et al., 1999). Our results support the idea that cis-regulatory divergence is the driving evolutionary mechanism behind the retention of the zebrafish *lhfpl5* ohnologs. Analysis of hair cell function in the different *lhfpl5* mutants agrees with the gene expression results, showing that *lhfpl5a* is required for transduction in the ear while *lhfpl5b* plays the same role in the lateral line organs. However, rescue of the MET channel defects in *lhfpl5b*^{vo35} mutants by GFP-tagged Lhfpl5a suggests that the functions of these ohnologs are at least partially interchangeable. This result is not surprising given the high degree of similarity between the Lhfpl5a and 5b proteins. As such, the subfunctionalization of the *lhfpl5* ohnologs appears to be caused by the divergence in their expression patterns rather than functional differences in their protein products. It is possible that a similar mechanism is responsible for the retention of both genes in other teleost species as well, though the expression patterns of the *lhfpl5* ohnologs has not been examined in other fish species.

425 The non-overlapping expression of the *lhfpl5* ohnologs provides us with a unique genetic tool to study
426 lateral line function. Most mechanotransduction mutants in zebrafish disrupt both inner ear and lateral
427 line hair cell function (Nicolson, 2017). As such, we are unable to assess the role of the lateral line
428 independently of auditory and vestibular defects, which are lethal for larval fish. Future studies will
429 leverage this subfunctionalization of the *lhfpl5* ohnologs to dissect out the behavioral, physiological
430 and neurological contributions of lateral line function using a genetic mutant, which has never been
431 possible before.

432 5.3 The molecular requirements for bundle localization of MET complex proteins differs 433 between mouse and zebrafish hair cells.

434 Our understanding of mechanotransduction at the molecular level is heavily informed by work done
435 using mouse cochlear hair cells. However, analysis of zebrafish inner ear and lateral line hair cells can
436 lead to a more complete picture of how vertebrate sensory hair cells form the MET complex. At their
437 core, the genetic and molecular bases for mechanotransduction are well conserved between mouse and
438 zebrafish hair cells. For example, the tip link proteins Cdh23 and Pcdh15a, MET channel subunits
439 Tmc1/2, Tmie, and Lhfpl5, along with additional factors such as Tomt , Cib2 and Myo7aa are all
440 necessary for MET channel function in both mice and fish (Cunningham et al., 2017; Erickson et al.,
441 2017; Giese et al., 2017; Gleason et al., 2009; Kawashima et al., 2011; Nicolson et al., 1998; Pacentine
442 and Nicolson, 2019; Senften et al., 2006; Siemens et al., 2004; Söllner et al., 2004; Xiong et al., 2012;
443 Zhao et al., 2014). However, while each of these factors are required for mechanotransduction in
444 vertebrate hair cells, the details of how they contribute to MET channel function may differ depending
445 on the particular type of hair cell or the vertebrate species. For example, Tmie is required for Tmc
446 localization to the hair bundle in zebrafish (Pacentine and Nicolson, 2019), but this does not appear to
447 be the case in mouse cochlear hair cells (Zhao et al., 2014).

448 Based on multiple lines of evidence gathered from mice, TMC1 and TMC2 have different requirements
449 for LHFPL5 regarding localization to the hair bundle (Beurg et al., 2015). Endogenous TMC1 is absent
450 from the bundle in LHFPL5-deficient cochlear hair cells with the remaining MET current mediated
451 through TMC2. Exogenously-expressed TMC2 is still targeted correctly in *Lhfpl5* mutants, but it was
452 not reported whether the same is true for exogenous TMC1, nor whether similar requirements hold for
453 vestibular hair cells. As such, the role of LHFPL5 in mechanotransduction is not clear: is LHFPL5
454 required primarily for targeting TMC1 to the hair bundle, or does LHFPL5 mediate MET channel
455 function in other ways?

456 For our study, we used stable transgenic lines expressing GFP-tagged Tmc1 and Tmc2b to show that
457 the Tmcs do not require Lhfpl5a for targeting to the stereocilia of zebrafish vestibular hair cells. Nor
458 is Lhfpl5b required for Tmc2b-GFP localization in the hair bundle of neuromast hair cells. The
459 occasional FM labeled-hair cell in *lhfpl5b* and *lhfpl5a/5b* mutant neuromasts is consistent with the
460 continued ability of the Tmcs to localize to the hair bundle. This observation is reminiscent of the
461 sporadic, low level of FM dye labeling in the cochlear hair cells of *Lhfpl5* mutant mice (György et al.,
462 2017). Partial compensation by yet another member of the *lhfpl* family remains as a possible
463 explanation for the remaining basal channel function. Lastly, we find that exogenous Tmc expression
464 does not rescue MET channel activity in either *lhfpl5* mutant zebrafish. Taken together, our results
465 support a Tmc-independent role for Lhfpl5 proteins in mechanotransduction.

466 What then is the role of LHFPL5 in vertebrate mechanotransduction? LHFPL5 and PCDH15 are known
467 to form a protein complex and regulate each other's localization to the site of mechanotransduction in
468 mouse cochlear hair cells (Ge et al., 2018; Mahendrasingam et al., 2017; Xiong et al., 2012). However,

469 their localization to the hair bundle is not completely dependent on one another. For example, tips links
470 are not completely lost in *Lhfpl5*$^{-/-}$ cochlear hair cells and exogenous overexpression of PCDH15
471 partially rescues the transduction defects in *Lhfpl5* mutant mice (Xiong et al., 2012). Similarly, a
472 detailed immunogold study in wild type and *Pcdh15*$^{-/-}$ cochlear hair cells showed that there are
473 PCDH15-dependent and PCDH15-independent sites of LHFPL5 localization (Mahendrasingam et al.,
474 2017). PCDH15 is required for stable LHFPL5 localization at the tips of ranked stereocilia in
475 association with the MET channel complex. However, LHFPL5 is still targeted to shaft and ankle links,
476 unranked stereocilia, and the kinocilium in P0-P3 inner and outer hair cells from both wild type and
477 *Pcdh15*$^{-/-}$ mutant mice (Mahendrasingam et al., 2017). Whether the kinocilial localization would
478 remain in mature cochlear hair cells is not known because the kinocilia degenerate by P8 in mice and
479 detailed LHFPL5 localization in vestibular hair cells (which retain their kinocilium) has not been
480 reported.

481 Zebrafish hair cells retain a kinocilium throughout their life, thus providing a different context in which
482 to examine Lhfpl5 localization. In wild type hair cells, GFP-Lhfpl5a is present at the tips of the shorter
483 ranked stereocilia, but the most robust signal is detected in the tallest stereocilia adjacent to the
484 kinocilium. In *pcdh15a* mutants, only this "kinocilial link"-like signal remains in the hair bundle. This
485 result is similar to the LHFPL5 localization reported at the tips of the tallest stereocilia of P3 cochlear
486 hair cells from wild type mice, a region where LHFPL5 would presumably not be associated with either
487 PCDH15 or the TMCs (Mahendrasingam et al., 2017). Since the kinocilium does not degenerate in
488 zebrafish hair cells, our results suggest that Lhfpl5a is normally targeted to these kinocilial links in
489 wild type cells and that its retention at this site does not require Pcdh15a. Thus, there are PCDH15-
490 dependent and PCDH15-independent mechanisms of LHFPL5 localization in both mouse and
491 zebrafish hair cells. These results suggest that LHFPL5 performs as-of-yet uncharacterized PCDH15-
492 independent functions as well.

493 Cdh23 is thought to form part of the linkages between the kinocilium and adjacent stereocilia, and
494 therefore may play a role in retaining Lhfpl5a at these sites. Consistent with this hypothesis, *cdh23*
495 mutants do not exhibit GFP-Lhfpl5a accumulation in stereocilia. Instead, GFP-Lhfpl5a is diffusely
496 distributed throughout the kinocilium. These data suggest that normal Lhfpl5a localization requires
497 both Pcdh15a and Cdh23 function, albeit in distinct ways. This result differs from previous reports
498 which found that Lhfpl5 still localized to the tips of stereocilia in CDH23-deficient cochlear hair cells
499 of mice. The same study also could not detect a biochemical interaction between Lhfpl5 and CDH23
500 via co-IP in heterologous cells (Xiong et al., 2012). Given these contrasting results for mouse and
501 zebrafish hair cells, it seems that the requirement for Cdh23 in the localization of LHFPL5 is not a
502 universal one.

503 Given the available biochemical evidence, it is possible that the association between Lhfpl5a and
504 Cdh23 is indirect through an as-of-yet unidentified protein or protein complex. Based on the defects in
505 GFP-Lhfpl5a localization in *myo7aa* mutants, Myo7aa is a candidate member of this uncharacterized
506 protein complex. Taken together, these results highlight the fact that, although all sensory hair cells
507 share many core genetic and biochemical features, there are important details that differ between the
508 various types of hair cells and between vertebrate species. Analyzing these differences will allow for
509 a more comprehensive understanding of vertebrate hair cell function and the underlying principles of
510 mechanotransduction.

511

512

6 Conflict of Interest

The authors declare that the research was conducted in the absence of any commercial or financial relationships that could be construed as a potential conflict of interest.

7 Author Contributions

TE and TN conceived and designed the study; TE, IVP, AV, and RC collected and analyzed the data, TE wrote the manuscript with Methods sections contributed by IVP and AV and editorial input from TN and IVP.

8 Funding

This study was supported by funding from the NIDCD (R01 DC013572 and DC013531 to T.N.) and from East Carolina University's Division of Research, Economic Development and Engagement (REDE), Thomas Harriot College of Arts and Science (THCAS), and Department of Biology (to T.E.)

9 Acknowledgments

We thank Eliot Smith for assistance with CRISPR-Cas9 knockout of *lhfpl5b*. We also thank Leah Snyder, Matthew Esqueda, and members of the Erickson lab for their assistance with animal husbandry.

10 References

Allendorf, F. W., and Thorgaard, G. H. (1984). "Tetraploidy and the Evolution of Salmonid Fishes," in *Evolutionary Genetics of Fishes* (Boston, MA: Springer US), 1–53. doi:10.1007/978-1-4684-4652-4_1.

Beurg, M., Xiong, W., Zhao, B., Müller, U., and Fettiplace, R. (2015). Subunit determination of the conductance of hair-cell mechanotransducer channels. *Proc. Natl. Acad. Sci.* 112, 1589–1594. doi:10.1073/pnas.1420906112.

Blanco-Sanchez, B., Clement, A., Fierro, J., Washbourne, P., and Westerfield, M. (2014). Complexes of Usher proteins preassemble at the endoplasmic reticulum and are required for trafficking and ER homeostasis. *Dis. Model. Mech.* 7, 547–559. doi:10.1242/dmm.014068.

Boëda, B., El-Amraoui, A., Bahloul, A., Goodyear, R., Daviet, L., Blanchard, S., et al. (2002). Myosin VIIa, harmonin and cadherin 23, three Usher I gene products that cooperate to shape the sensory hair cell bundle. *EMBO J.* 21, 6689–99. doi:10.1093/emboj/cdf689.

Braasch, I., Gehrke, A. R., Smith, J. J., Kawasaki, K., Manousaki, T., Pasquier, J., et al. (2016). The spotted gar genome illuminates vertebrate evolution and facilitates human-teleost comparisons. *Nat. Genet.* 48, 427–437. doi:10.1038/ng.3526.

Chou, S.-W., Chen, Z., Zhu, S., Davis, R. W., Hu, J., Liu, L., et al. (2017). A molecular basis for water motion detection by the mechanosensory lateral line of zebrafish. *Nat. Commun.* 8, 2234. doi:10.1038/s41467-017-01604-2.

Cunningham, C. L., and Müller, U. (2019). Molecular Structure of the Hair Cell Mechanoelectrical

549 Transduction Complex. *Cold Spring Harb. Perspect. Med.* 9, a033167.
550 doi:10.1101/cshperspect.a033167.

551 Cunningham, C. L., Wu, Z., Jafari, A., Zhao, B., Schrode, K., Harkins-Perry, S., et al. (2017). The
552 murine catecholamine methyltransferase mTOMT is essential for mechanotransduction by
553 cochlear hair cells. *Elife* 6. doi:10.7554/eLife.24318.

554 Dereeper, A., Guignon, V., Blanc, G., Audic, S., Buffet, S., Chevenet, F., et al. (2008). Phylogeny.fr:
555 robust phylogenetic analysis for the non-specialist. *Nucleic Acids Res.* 36, W465–W469.
556 doi:10.1093/nar/gkn180.

557 Erickson, T., French, C. R., and Waskiewicz, A. J. (2010). Meis1 specifies positional information in
558 the retina and tectum to organize the zebrafish visual system. *Neural Dev.* 5, 22.
559 doi:10.1186/1749-8104-5-22.

560 Erickson, T., Morgan, C. P., Olt, J., Hardy, K., Busch-Nentwich, E., Maeda, R., et al. (2017).
561 Integration of Tmc1/2 into the mechanotransduction complex in zebrafish hair cells is regulated
562 by Transmembrane O-methyltransferase (Tomt). *Elife* 6. doi:10.7554/eLife.28474.

563 Ernest, S., Rauch, G.-J., Haffter, P., Geisler, R., Petit, C., and Nicolson, T. (2000). Mariner is
564 defective in myosin VIIA: a zebrafish model for human hereditary deafness. *Hum. Mol. Genet.*
565 9, 2189–2196. doi:10.1093/hmg/9.14.2189.

566 Force, A., Lynch, M., Pickett, F. B., Amores, A., Yan, Y. L., and Postlethwait, J. (1999).
567 Preservation of duplicate genes by complementary, degenerative mutations. *Genetics* 151,
568 1531–45. Available at: http://www.ncbi.nlm.nih.gov/pubmed/10101175 [Accessed September
569 14, 2018].

570 Gagnon, J. A., Valen, E., Thyme, S. B., Huang, P., Ahkmetova, L., Pauli, A., et al. (2014). Efficient
571 Mutagenesis by Cas9 Protein-Mediated Oligonucleotide Insertion and Large-Scale Assessment
572 of Single-Guide RNAs. *PLoS One* 9, e98186. doi:10.1371/journal.pone.0098186.

573 Ge, J., Elferich, J., Goehring, A., Zhao, H., Schuck, P., and Gouaux, E. (2018). Structure of mouse
574 protocadherin 15 of the stereocilia tip link in complex with LHFPL5. *Elife* 7.
575 doi:10.7554/eLife.38770.

576 Giese, A. P. J., Tang, Y.-Q., Sinha, G. P., Bowl, M. R., Goldring, A. C., Parker, A., et al. (2017).
577 CIB2 interacts with TMC1 and TMC2 and is essential for mechanotransduction in auditory hair
578 cells. *Nat. Commun.* 8, 43. doi:10.1038/s41467-017-00061-1.

579 Gleason, M. R., Nagiel, A., Jamet, S., Vologodskaia, M., López-Schier, H., and Hudspeth, A. J.
580 (2009). The transmembrane inner ear (Tmie) protein is essential for normal hearing and balance
581 in the zebrafish. *Proc. Natl. Acad. Sci. U. S. A.* 106, 21347–52. doi:10.1073/pnas.0911632106.

582 Goodyear, R. J., Forge, A., Legan, P. K., and Richardson, G. P. (2010). Asymmetric distribution of
583 cadherin 23 and protocadherin 15 in the kinocilial links of avian sensory hair cells. *J. Comp.*
584 *Neurol.* 518, 4288–4297. doi:10.1002/cne.22456.

585 György, B., Sage, C., Indzhykulian, A. A., Scheffer, D. I., Brisson, A. R., Tan, S., et al. (2017).
586 Rescue of Hearing by Gene Delivery to Inner-Ear Hair Cells Using Exosome-Associated AAV.

587 *Mol. Ther.* 25, 379–391. doi:10.1016/j.ymthe.2016.12.010.

588 Kawashima, Y., Géléoc, G. S. G., Kurima, K., Labay, V., Lelli, A., Asai, Y., et al. (2011).
589 Mechanotransduction in mouse inner ear hair cells requires transmembrane channel-like genes.
590 *J. Clin. Invest.* 121, 4796–809. doi:10.1172/JCI60405.

591 Kazmierczak, P., Sakaguchi, H., Tokita, J., Wilson-Kubalek, E. M., Milligan, R. A., Müller, U., et al.
592 (2007). Cadherin 23 and protocadherin 15 interact to form tip-link filaments in sensory hair
593 cells. *Nature* 449, 87–91. doi:10.1038/nature06091.

594 Lefevre, G., Michel, V., Weil, D., Lepelletier, L., Bizard, E., Wolfrum, U., et al. (2008). A core
595 cochlear phenotype in USH1 mouse mutants implicates fibrous links of the hair bundle in its
596 cohesion, orientation and differential growth. *Development* 135, 1427–1437.
597 doi:10.1242/dev.012922.

598 Li, X., Yu, X., Chen, X., Liu, Z., Wang, G., Li, C., et al. (2019). Localization of TMC1 and LHFPL5
599 in auditory hair cells in neonatal and adult mice. *FASEB J.* 33, 6838–6851.
600 doi:10.1096/fj.201802155RR.

601 Longo-Guess, C. M., Gagnon, L. H., Cook, S. A., Wu, J., Zheng, Q. Y., and Johnson, K. R. (2005). A
602 missense mutation in the previously undescribed gene Tmhs underlies deafness in hurry-scurry
603 (hscy) mice. *Proc. Natl. Acad. Sci.* 102, 7894–7899. doi:10.1073/pnas.0500760102.

604 Lu, Z., and DeSmidt, A. A. (2013). Early Development of Hearing in Zebrafish. *JARO J. Assoc. Res.*
605 *Otolaryngol.* 14, 509. doi:10.1007/S10162-013-0386-Z.

606 Lv, C., Stewart, W. J., Akanyeti, O., Frederick, C., Zhu, J., Santos-Sacchi, J., et al. (2016). Synaptic
607 Ribbons Require Ribeye for Electron Density, Proper Synaptic Localization, and Recruitment of
608 Calcium Channels. *Cell Rep.* 15, 2784–2795. doi:10.1016/j.celrep.2016.05.045.

609 Maeda, R., Kindt, K. S., Mo, W., Morgan, C. P., Erickson, T., Zhao, H., et al. (2014). Tip-link
610 protein protocadherin 15 interacts with transmembrane channel-like proteins TMC1 and TMC2.
611 *Proc. Natl. Acad. Sci. U. S. A.* 111, 12907–12. doi:10.1073/pnas.1402152111.

612 Maeda, R., Pacentine, I. V., Erickson, T., and Nicolson, T. (2017). Functional Analysis of the
613 Transmembrane and Cytoplasmic Domains of Pcdh15a in Zebrafish Hair Cells. *J. Neurosci.* 37,
614 3231–3245. doi:10.1523/JNEUROSCI.2216-16.2017.

615 Mahendrasingam, S., Fettiplace, R., Alagramam, K. N., Cross, E., and Furness, D. N. (2017).
616 Spatiotemporal changes in the distribution of LHFPL5 in mice cochlear hair bundles during
617 development and in the absence of PCDH15. *PLoS One* 12, e0185285.
618 doi:10.1371/journal.pone.0185285.

619 Morgan, C. P., Krey, J. F., Grati, M., Zhao, B., Fallen, S., Kannan-Sundhari, A., et al. (2016).
620 PDZD7-MYO7A complex identified in enriched stereocilia membranes. *Elife* 5.
621 doi:10.7554/eLife.18312.

622 Nicolson, T. (2017). The genetics of hair-cell function in zebrafish. *J. Neurogenet.* 31, 102–112.
623 doi:10.1080/01677063.2017.1342246.

624 Nicolson, T., Rüsch, A., Friedrich, R. W., Granato, M., Ruppersberg, J. P., and Nüsslein-Volhard, C.
625 (1998). Genetic analysis of vertebrate sensory hair cell mechanosensation: the zebrafish circler
626 mutants. *Neuron* 20, 271–83. doi:10.1016/S0896-6273(00)80455-9.

627 Obholzer, N., Swinburne, I. A., Schwab, E., Nechiporuk, A. V, Nicolson, T., and Megason, S. G.
628 (2012). Rapid positional cloning of zebrafish mutations by linkage and homozygosity mapping
629 using whole-genome sequencing. *Development* 139, 4280–4290. doi:10.1242/dev.083931.

630 Ohno, S. (1970). *Evolution by Gene Duplication*. Berlin, Heidelberg: Springer Berlin Heidelberg
631 doi:10.1007/978-3-642-86659-3.

632 Pacentine, I. V., and Nicolson, T. (2019). Subunits of the mechano-electrical transduction channel,
633 Tmc1/2b, require Tmie to localize in zebrafish sensory hair cells. *PLOS Genet.* 15, e1007635.
634 doi:10.1371/journal.pgen.1007635.

635 Pan, B., Akyuz, N., Liu, X.-P., Asai, Y., Nist-Lund, C., Kurima, K., et al. (2018). TMC1 Forms the
636 Pore of Mechanosensory Transduction Channels in Vertebrate Inner Ear Hair Cells. *Neuron* 99,
637 736-753.e6. doi:10.1016/j.neuron.2018.07.033.

638 Pan, B., Géléoc, G. S., Asai, Y., Horwitz, G. C., Kurima, K., Ishikawa, K., et al. (2013). TMC1 and
639 TMC2 Are Components of the Mechanotransduction Channel in Hair Cells of the Mammalian
640 Inner Ear. *Neuron* 79, 504–515. doi:10.1016/j.neuron.2013.06.019.

641 R Core Team (2019). R: A Language and Environment for Statistical Computing. Available at:
642 https://www.r-project.org/.

643 RStudio Team (2018). RStudio: Integrated Development Environment for R. Available at:
644 http://www.rstudio.com/.

645 Schneider, C. A., Rasband, W. S., and Eliceiri, K. W. (2012). NIH Image to ImageJ: 25 years of
646 image analysis. *Nat. Methods* 9, 671–5. Available at:
647 http://www.ncbi.nlm.nih.gov/pubmed/22930834 [Accessed January 13, 2019].

648 Seiler, C., Ben-David, O., Sidi, S., Hendrich, O., Rusch, A., Burnside, B., et al. (2004). Myosin VI is
649 required for structural integrity of the apical surface of sensory hair cells in zebrafish. *Dev. Biol.*
650 272, 328–38. doi:10.1016/j.ydbio.2004.05.004.

651 Seiler, C., Finger-Baier, K. C., Rinner, O., Makhankov, Y. V, Schwarz, H., Neuhauss, S. C. F., et al.
652 (2005). Duplicated genes with split functions: independent roles of protocadherin15 orthologues
653 in zebrafish hearing and vision. *Development* 132, 615–23. doi:10.1242/dev.01591.

654 Senften, M., Schwander, M., and Kazmierczak, P. (2006). Physical and functional interaction
655 between protocadherin 15 and myosin VIIa in mechanosensory hair cells. *J.* 26, 2060–2071.
656 doi:10.1523/JNEUROSCI.4251-05.2006.

657 Shabbir, M. I., Ahmed, Z. M., Khan, S. Y., Riazuddin, S., Waryah, A. M., Khan, S. N., et al. (2006).
658 Mutations of human TMHS cause recessively inherited non-syndromic hearing loss. *J. Med.*
659 *Genet.* 43, 634–40. doi:10.1136/jmg.2005.039834.

660 Sheets, L., Trapani, J. G., Mo, W., Obholzer, N., and Nicolson, T. (2011). Ribeye is required for

661 presynaptic CaV1.3a channel localization and afferent innervation of sensory hair cells.
662 *Development* 138, 1309–1319. doi:10.1242/dev.059451.

663 Sidi, S., Busch-Nentwich, E., Friedrich, R., Schoenberger, U., and Nicolson, T. (2004). gemini
664 encodes a zebrafish L-type calcium channel that localizes at sensory hair cell ribbon synapses. *J.*
665 *Neurosci.* 24, 4213–4223. doi:10.1523/JNEUROSCI.0223-04.2004.

666 Siemens, J., Lillo, C., Dumont, R. A., Reynolds, A., Williams, D. S., Gillespie, P. G., et al. (2004).
667 Cadherin 23 is a component of the tip link in hair-cell stereocilia. *Nature* 428, 950–955.
668 doi:10.1038/nature02483.

669 Singh, P. P., and Isambert, H. (2019). OHNOLOGS v2: A comprehensive resource for the genes
670 retained from whole genome duplication in vertebrates. *bioRxiv*, 717124. doi:10.1101/717124.

671 Söllner, C., Rauch, G.-J., Siemens, J., Geisler, R., Schuster, S. C., Müller, U., et al. (2004). Mutations
672 in cadherin 23 affect tip links in zebrafish sensory hair cells. *Nature* 428, 955–959.
673 doi:10.1038/nature02484.

674 Thisse, C., and Thisse, B. (2008). High-resolution in situ hybridization to whole-mount zebrafish
675 embryos. *Nat. Protoc.* 3, 59–69. doi:10.1038/nprot.2007.514.

676 Westerfield, M. (2000). *The zebrafish book. A guide for the laboratory use of zebrafish (Danio*
677 *rerio).* 4th ed. Eugene OR: University of Oregon Available at:
678 http://zfin.org/zf_info/zfbook/zfbk.html.

679 Wickham, H. (2016). *ggplot2: Elegant Graphics for Data Analysis*. Springer-Verlag New York
680 Available at: https://ggplot2.tidyverse.org.

681 Wolfe, K. (2000). Robustness—it's not where you think it is. *Nat. Genet.* 25, 3–4.
682 doi:10.1038/75560.

683 Xiong, W., Grillet, N., Elledge, H. M., Wagner, T. F. J., Zhao, B., Johnson, K. R., et al. (2012).
684 TMHS is an integral component of the mechanotransduction machinery of cochlear hair cells.
685 *Cell* 151, 1283–95. doi:10.1016/j.cell.2012.10.041.

686 Yao, Q., DeSmidt, A. A., Tekin, M., Liu, X., and Lu, Z. (2016). Hearing Assessment in Zebrafish
687 During the First Week Postfertilization. *Zebrafish* 13, 79. doi:10.1089/ZEB.2015.1166.

688 Zhao, B., Wu, Z., Grillet, N., Yan, L., Xiong, W., Harkins-Perry, S., et al. (2014). TMIE Is an
689 Essential Component of the Mechanotransduction Machinery of Cochlear Hair Cells. *Neuron*
690 84, 954–967. doi:10.1016/j.neuron.2014.10.041.

691 Zou, J., Chen, Q., Almishaal, A., Mathur, P. D., Zheng, T., Tian, C., et al. (2017). The roles of USH1
692 proteins and PDZ domain-containing USH proteins in USH2 complex integrity in cochlear hair
693 cells. *Hum. Mol. Genet.* 26, 624–636. doi:10.1093/hmg/ddw421.

694

695

696

11 Figure legends

Figure 1. Duplicated *lhfpl5* genes in teleost fish. (**A**) Phylogenic tree of representative teleost and vertebrate Lhfpl5 protein sequences. See Supplemental Table 1 for species' names and protein accession numbers. (**B**) Sequence alignment of Lhfpl5 proteins from zebrafish (*Danio rerio*, Dr), chicken (*Gallus gallus*, Gg), mouse (*Mus musculus*, Mm), and humans (*Homo sapiens*, Hs). Regions of the proteins coded for by exons 1 and 3 are shaded grey. Locations of the transmembrane (TM) helices 1-4 are shown in the linear protein structure diagram. The *lhfpl5a*^{tm290d} and *lhfpl5b*^{vo35} mutations are indicated by the red triangle and red square, respectively.

Figure 2. Zebrafish *lhfpl5a* and *lhfpl5b* genes are expressed in distinct populations of sensory hair cells. Whole mount mRNA *in situ* hybridization for *lhfpl5a* (**A, C, E, G, I**) and *lhfpl5b* (**B, D, F, H, J**) at 1, 2, and 5 days post-fertilization (dpf). Panels G-J are details from 5 dpf larvae. Abbreviations: NMs = neuromasts, HC = hair cell, SC = support cell. Scale bars: A, B = 50 µm; C-F = 100 µm; G-J = 25 µm.

Figure 3. *lhfpl5a* is required for auditory and vestibular hair cell function. (**A**) Boxplot showing the first peak amplitude (µV) of microphonic recordings from the inner ear of 3 dpf wild type, *lhfpl5a*^{tm290d}, and *lhfpl5b*^{vo35} larvae. The boxes cover the inter-quartile range (IQR), and the whiskers represent the minimum and maximum datapoints within 1.5 times the IQR. Values from individual larvae are indicated by the black dots and outliers indicated by a diamond. Asterisks indicate $p < 0.01$ (**) by Welch's t-test. ns = not significant. (**B**) Boxplot of the acoustic startle response in 6 dpf wild type and *lhfpl5a*^{tm290d} mutants, with or without the *GFP-lhfpl5a*^{vo23Tg} transgene. Values from individual larvae are indicated by the black dots and outliers indicated by a diamond. Asterisks indicate $p < 0.001$ (***) by Welch's t-test. ns = not significant. (**C-F'**) FM 4-64 dye labeling assay for MET channel activity in the lateral cristae of wild type and *lhfpl5a*^{tm290d} mutants, with or without the *GFP-lhfpl5a*^{vo23Tg} transgene. G' and H' are images of GFP-Lhfpl5a protein in the bundle of the hair cells shown above in panels G and H. n = 2, 3, 12, and 4 for the genotypes in panels C-F, respectively. Scale bars = 5 µm and apply to all images.

Figure 4. *lhfpl5b* is required for lateral line hair cell function. (**A-C**) Representative images of 5 dpf zebrafish larvae labeled with the MET channel-permeant dye FM 1-43. (**D-G**) Representative images of individual neuromasts from 2 dpf and 5 dpf wild type and *lhfpl5b*^{vo35} larvae labeled with FM 1-43. Dashed lines outline the cluster of hair cells in each neuromast. (**H**) Quantification of normalized FM 1-43 fluorescence intensity per hair cell of 2 dpf and 5 dpf neuromasts (n = 10 WT, 14 *lhfpl5b*^{vo35} NMs at 2 dpf; n = 6 WT, 13 *lhfpl5b*^{vo35} NMs each genotype at 5 dpf). The box plots cover the inter-quartile range (IQR), and the whiskers represent the minimum and maximum datapoints within 1.5 times the IQR. Asterisks indicate $p < 0.001$ (***) by Welch's t-test. (**I**) Quantification of hair cell number in L1, MI1, and O2 neuromasts in 5 dpf *lhfpl5b*^{vo35} mutants and wild-type siblings expressing the *vo68Tg* hair cell GFP transgene. The box plots are the same as in H. Asterisks indicate $p < 0.05$ (*) and $p < 0.01$ (**) by Welch's t-test. (**J, K**) Rescue of FM dye labeling in *lhfpl5b*^{vo35} mutants by the *GFP-lhfpl5a*^{vo23Tg} transgene. The GFP-Lhfpl5a bundle and FM 4–64 images are from the same NM for each genotype. Scale bars = 5 µm, applies to panels D-G, J, K; 2 µm in J, K insets).

Figure 5. Tmc proteins do not require Lhfpl5a or Lhfpl5b for localization to the stereocilia of zebrafish hair cells. (**A – D'**) Representative images of Tmc1-GFP (*vo27Tg*) or Tmc2b-GFP (*vo28Tg*) in the lateral cristae of wild type (**A, A', C, C'**) and *lhfpl5a*^{tm290d} (**B, B', D, D'**) larvae. The GFP-only channel is shown in panels A - D and overlaid with a light image of the bundles in A' - D'. (**E – F'**) Representative images of Tmc2b-GFP (*vo28Tg*) in the neuromasts of wild type (**E, E'**) and *lhfpl5b*^{vo35}

741 (**F, F'**) larvae. The GFP-only channel is shown in panels E and F and overlaid with a light image of
742 the bundles in E' and F'. Scale bars = 3 µm in all panels.

743 **Figure 6.** Lhfpl5a requires MET complex proteins Pcdh15a, Cdh23, and Myo7a for normal localization
744 in the stereocilia of zebrafish hair cells. (**A, B**) Immunostain of Pcdh15a (magenta) in the lateral cristae
745 of wild type and *lhfpl5a*^{tm290d} mutants at 3 dpf. Phalloidin-stained actin of the hair bundle is shown in
746 green. Arrows indicate areas of Pcdh15a accumulation. (**C-F'**) Representative images of GFP-Lhfpl5a
747 (*vo23Tg*) in the lateral cristae hair bundles of wild type (**C, C'**) and *pcdh15a*^{psi7} (**D, D'**), *cdh23*^{nl9} (**E,**
748 **E'**), and *myo7aa*^{ty220} (**F, F'**) mutants. White arrows indicate GFP signal in the presumptive kinocilial
749 linkages, yellow arrow heads indicate GFP signal in the stereocilia or the base of the hair bundle, and
750 brackets indicate GFP signal in the kinocilium. Scale bars = 3 µm in A, B; 2 µm in C-F'.

751

752 **Figure 1**

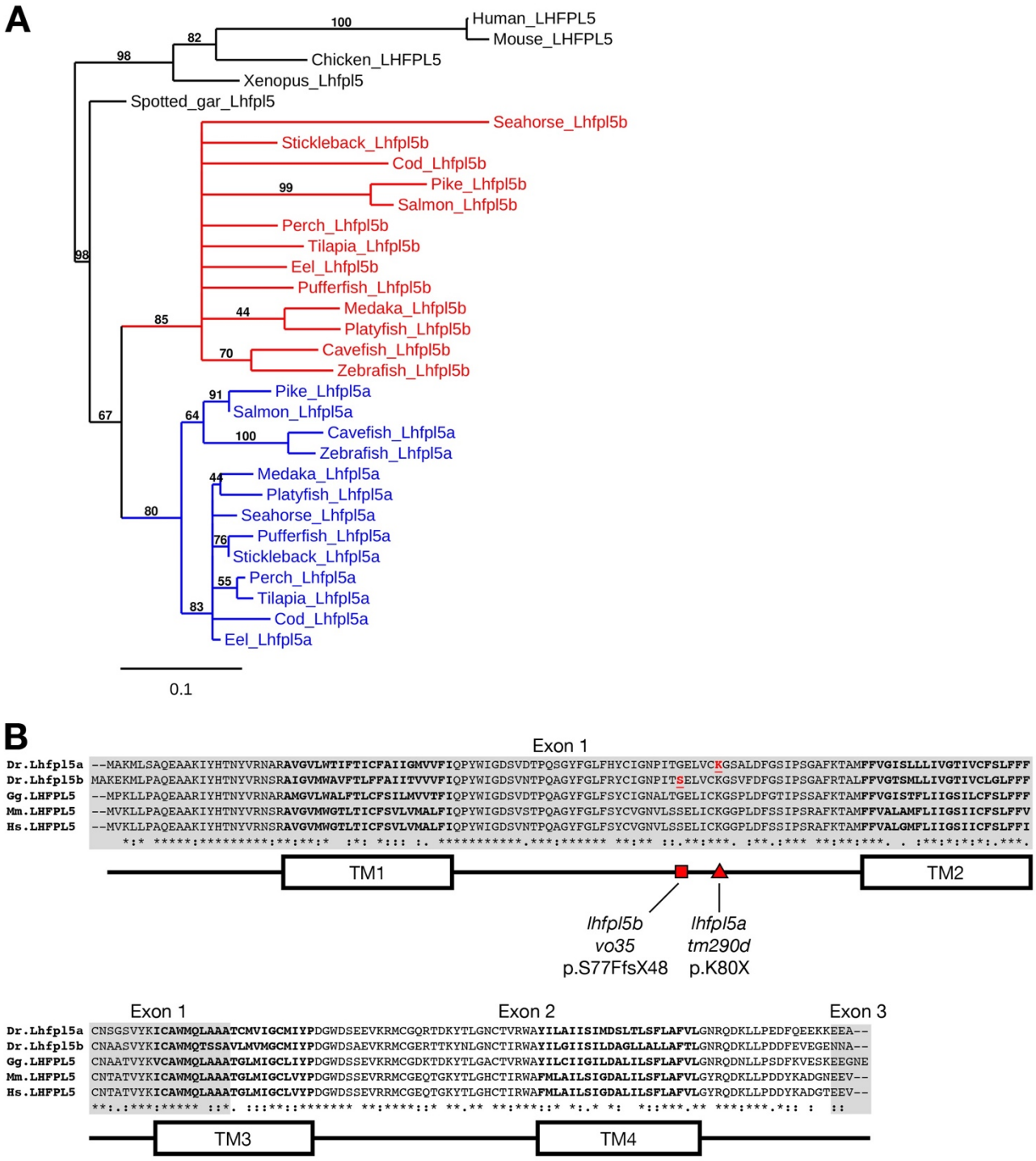
A
Human_LHFPL5
Mouse_LHFPL5
Chicken_LHFPL5
Xenopus_Lhfpl5
Spotted_gar_Lhfpl5
Seahorse_Lhfpl5b
Stickleback_Lhfpl5b
Cod_Lhfpl5b
Pike_Lhfpl5b
Salmon_Lhfpl5b
Perch_Lhfpl5b
Tilapia_Lhfpl5b
Eel_Lhfpl5b
Pufferfish_Lhfpl5b
Medaka_Lhfpl5b
Platyfish_Lhfpl5b
Cavefish_Lhfpl5b
Zebrafish_Lhfpl5b
Pike_Lhfpl5a
Salmon_Lhfpl5a
Cavefish_Lhfpl5a
Zebrafish_Lhfpl5a
Medaka_Lhfpl5a
Platyfish_Lhfpl5a
Seahorse_Lhfpl5a
Pufferfish_Lhfpl5a
Stickleback_Lhfpl5a
Perch_Lhfpl5a
Tilapia_Lhfpl5a
Cod_Lhfpl5a
Eel_Lhfpl5a
0.1
B
Exon 1
Dr.Lhfpl5a --MAKMLSAQEAAKIYHTNYVRNARAVGVLWTIFTICFAIIGMVVFIQPYWIGDSVDTPQSGYFGLFHYCIGNPITGELVCKGSALDFGSIPSGAFKTAMFFVGISLLLIVGTIVCFSLFFF
Dr.Lhfpl5b MAKEKMLPAQEAAKIYHTNYVRNSRAIGVMWAVFTLFFAIITVVVFIQPYWIGDSVNTPQAGYFGLFRYCIGNPITSELVCKGSVFDFGSIPSGAFRTALFFVGTSMLLIVGTIVCLGLFFF
Gg.LHFPL5 --MPKLLPAQEAARIYHTNYVRNARAMGVLWALFTLCFSILMVVTFIQPYWIGDSVDTPQAGYFGLFSYCIGNALTGELICKGSPLDFGTIPSSAFKTAMFFVGISTFLIIGSILCFSLFFF
Mm.LHFPL5 --MVKLLPAQEAAKIYHTNYVRNSRAVGVMWGTLTICFSVLVMALFIQPYWIGDSVSTPQAGYFGLFSYCVGNVLSSELICKGGPLDFSSIPSRAFKTAMFFVALAMFLIIGSIICFSLFFV
Hs.LHFPL5 --MVKLLPAQEAAKIYHTNYVRNSRAVGVMWGTLTICFSVLVMALFIQPYWIGDSVNTPQAGYFGLFSYCVGNVLSSELICKGGPLDFSSIPSRAFKTAMFFVALGMFLIIGSIICFSLFFI
TM1
TM2
lhfpl5b vo35 p.S77FfsX48
lhfpl5a tm290d p.K80X
Exon 1
Exon 2
Exon 3
Dr.Lhfpl5a CNSGSVYKICAWMQLAAATCMVIGCMIYPDGWDSEEVKRMCGQRTDKYTLGNCTVRWAYILAIISIMDSLTLSFLAFVLGNRQDKLLPEDFQEEKKEEA--
Dr.Lhfpl5b CNAASVYKICAWMQTSSAVLMVMGCMIYPDGWDSAEVKRMCGERTTKYNLGNCTIRWAYILGIISILDAGLLALLAFTLGNRQDKLLPDDFEVEGENNA--
Gg.LHFPL5 CNAATVYKVCAWMQLAAATGLMIGCLIYPDGWDSSEVKRMCGDKTDKYTLGACTVRWAYILCIIGILDALILSFLAFVLGNRQDNLLPSDFKVESKEEGNE
Mm.LHFPL5 CNTATVYKICAWMQLAAATGLMIGCLVYPDGWDSSEVRRMCGEQTGKYTLGHCTIRWAFMLAILSIGDALILSFLAFVLGYRQDKLLPDDYKADGNEEV--
Hs.LHFPL5 CNTATVYKICAWMQLAAATGLMIGCLVYPDGWDSSEVRRMCGEQTGKYTLGHCTIRWAFMLAILSIGDALILSFLAFVLGYRQDKLLPDDYKADGTEEV--
TM3
TM4

753 **Figure 2**

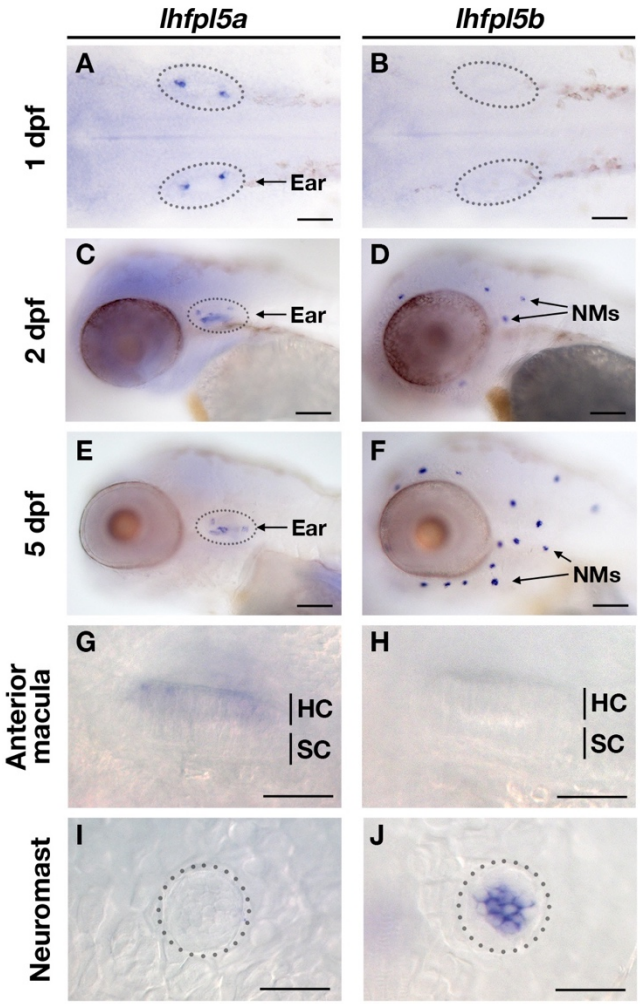

754

755

Figure 3

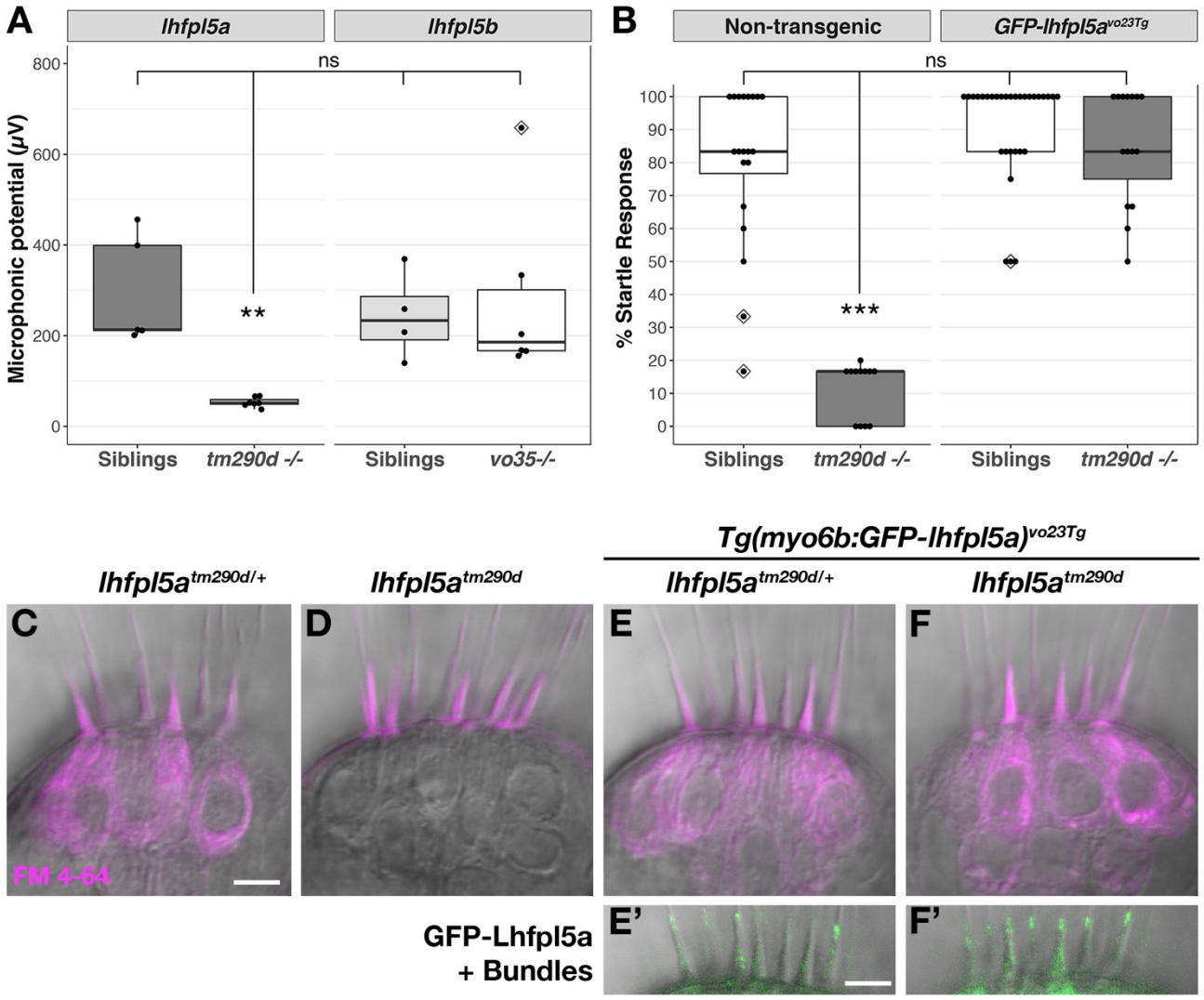
A
lhfpl5a
lhfpl5b
ns
**
Microphonic potential (μV)
800
600
400
200
0
Siblings
tm290d -/-
Siblings
vo35-/-
B
Non-transgenic
GFP-lhfpl5a vo23Tg
ns
***
% Startle Response
100
90
80
70
60
50
40
30
20
10
0
Siblings
tm290d -/-
Siblings
tm290d -/-
Tg(myo6b:GFP-lhfpl5a)vo23Tg
lhfpl5a tm290d/+
lhfpl5a tm290d
lhfpl5a tm290d/+
lhfpl5a tm290d
C
D
E
F
FM 4-64
GFP-Lhfpl5a
+ Bundles
E'
F'

759 **Figure 4**

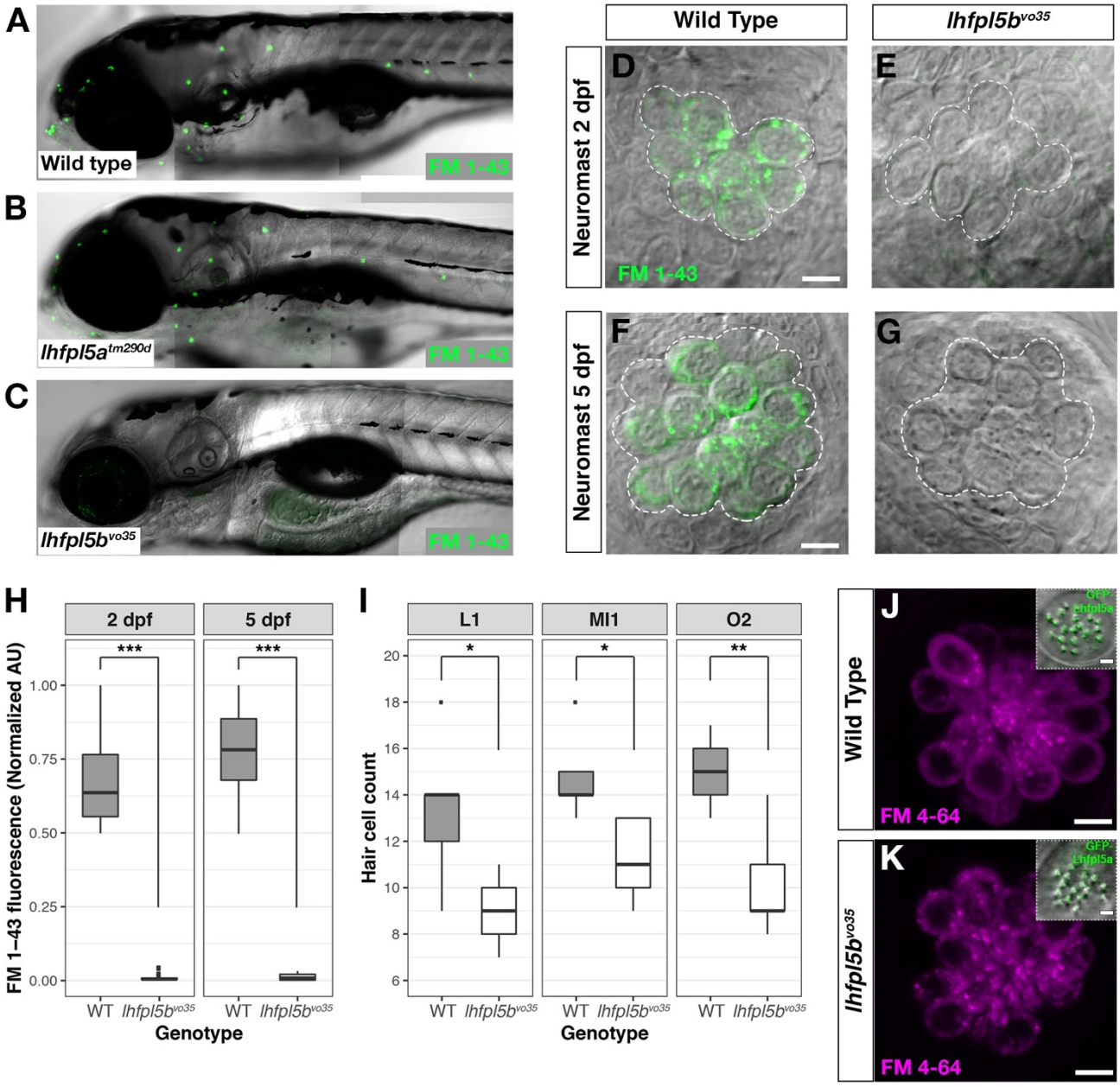

760

761

762 **Figure 5**

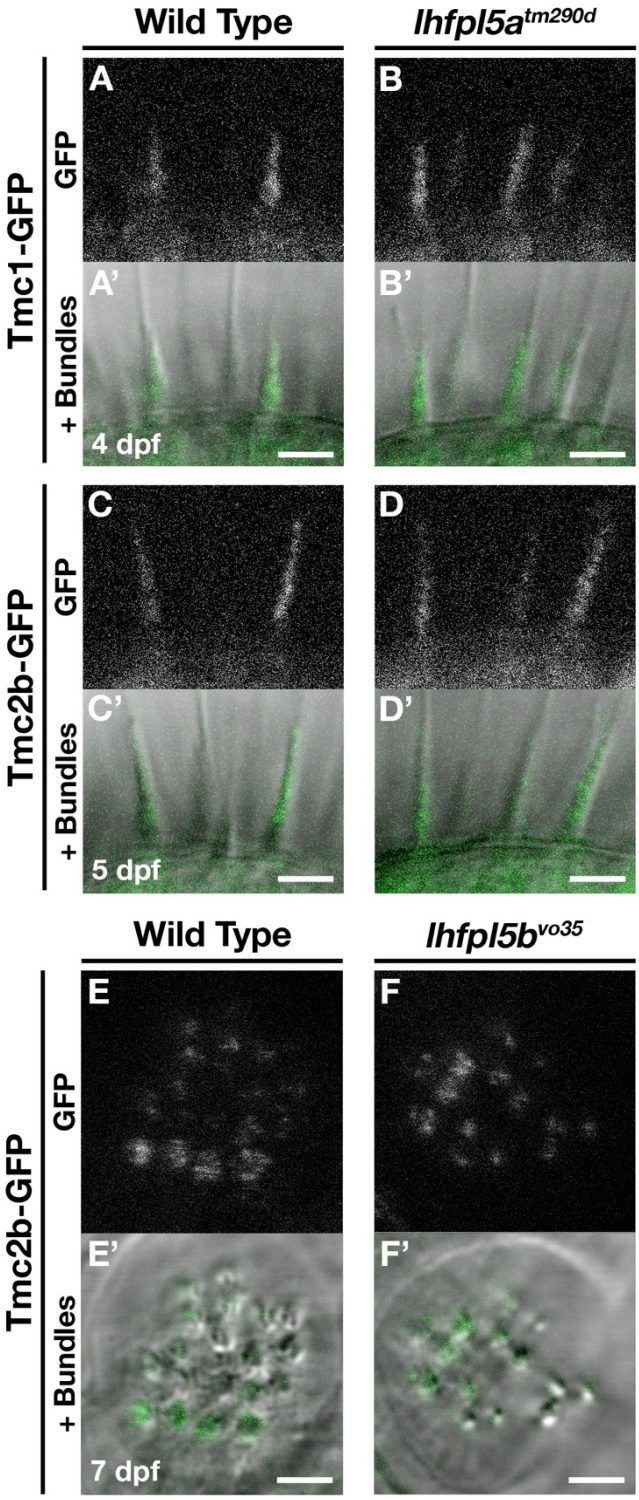

785

786 **Figure 6**

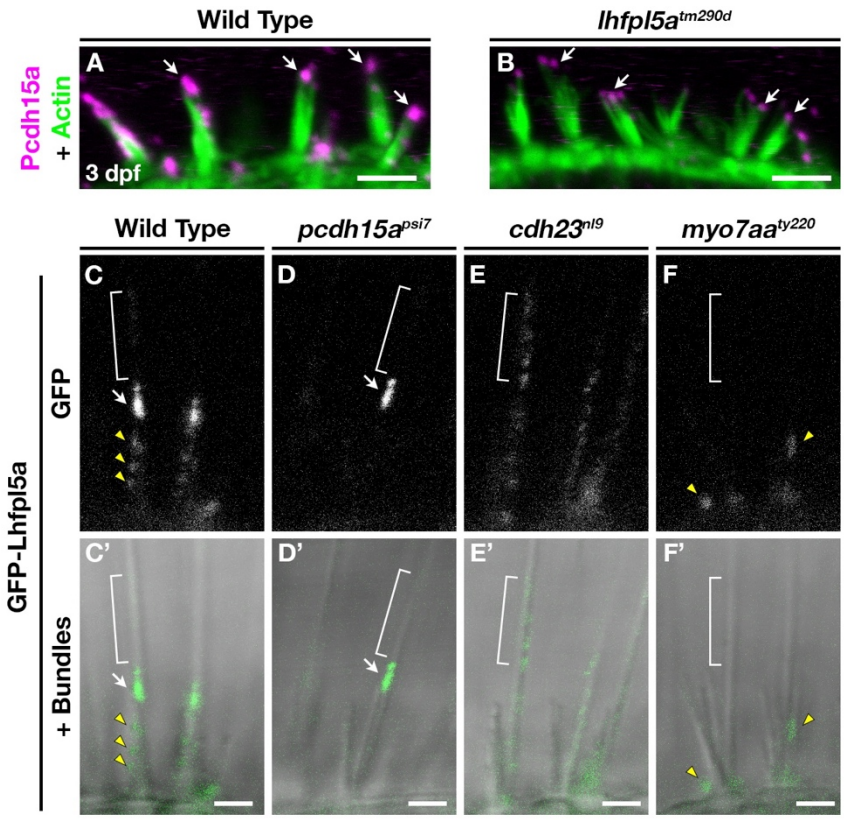

799

800

801 **Supplemental Table 1.** Lhfpl5 proteins used to construct the phylogenetic tree in Figure 1A.

Common name	Species	Phylogenetic Order	Gene	Accession number
Seahorse	*Hippocampus comes*	Syngnathiformes	*lhfpl5a*	XP_019736131.1
			lhfpl5b	XP_019716386.1
Salmon (Atlantic)	*Salmo salar*	Salmoniformes	*lhfpl5a*	XP_014021466.1
			lhfpl5b	XP_014002848.1
Pufferfish	*Takifugu rubripes*	Tetraodontiformes	*lhfpl5a*	ENSTRUP00000020283.2
			lhfpl5b	ENSTRUP00000041734.2
Platyfish	*Xiphophorus maculatus*	Cyprinodontiformes	*lhfpl5a*	ENSXMAP00000020967.1
			lhfpl5b	ENSXMAP00000010306.1
Medaka	*Oryzias latipes*	Beloniformes	*lhfpl5a*	ENSORLP00000042616.1
			lhfpl5b	ENSORLP00000008018.2
Zebrafish	*Danio rerio*	Cypriniformes	*lhfpl5a*	ENSDARP00000066188.3
			lhfpl5b	ENSDARP00000073423.4
Cavefish (Blind)	*Astyanax mexicanus*	Characiformes	*lhfpl5a*	ENSAMXP00000035004.1
			lhfpl5b	ENSAMXP00000007271.2
Stickleback (3-spine)	*Gasterosteus aculeatus*	Gasterosteiformes	*lhfpl5a*	ENSGACP00000010149.1
			lhfpl5b	ENSGACP00000010766.1
Tilapia	*Oreochromis niloticus*	Cichliformes	*lhfpl5a*	ENSONIP00000024352.1
			lhfpl5b	ENSONIP00000014897.1
Perch (Climbing)	*Anabas testudineus*	Perciformes	*lhfpl5a*	ENSATEP00000035217.1
			lhfpl5b	ENSATEP00000029406.1
Eel (Zig-zag)	*Mastacembelus armatus*	Synbranchiformes	*lhfpl5a*	ENSMAMP00000013383.1
			lhfpl5b	ENSMAMP00000016042.1
Cod	*Gadus morhua*	Gadiformes	*lhfpl5a*	ENSGMOP00000012109.1
			lhfpl5b	ENSGMOP00000016613.1
Pike (Northern)	*Esox lucius*	Esociformes	*lhfpl5a*	ENSELUP00000020567.1
			lhfpl5b	ENSELUP00000014071.1
Spotted gar	*Lepisosteus oculatus*	Lepisosteiformes	*lhfpl5*	ENSLOCP00000013703.1
Xenopus	*Xenopus tropicalis*	Anura	*lhfpl5*	ENSXETP00000058779.1
Chicken	*Gallus gallus*	Galliformes	*lhfpl5*	ENSGALP00000053562.1
Mouse	*Mus musculus*	Rodentia	*lhfpl5*	ENSMUSP00000156557.1
Human	*Homo sapiens*	Primates	*lhfpl5*	ENSP00000493955.1

802

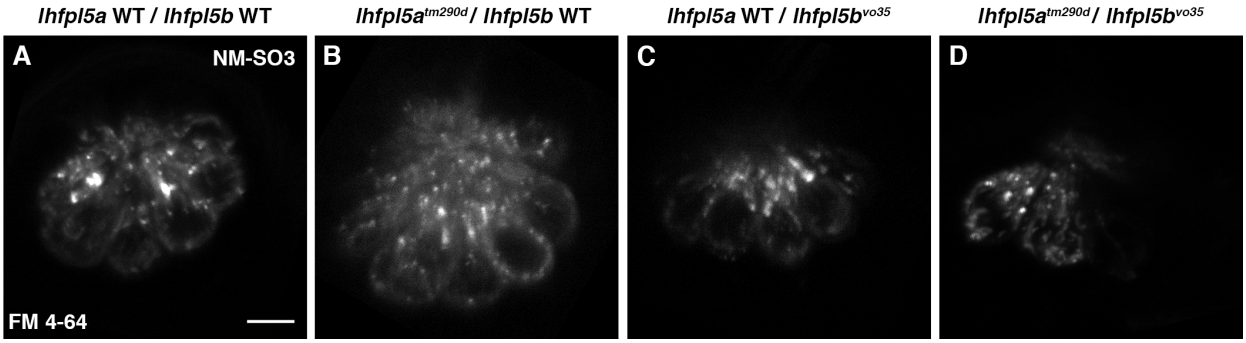

Supplemental Figure 1. Examples of residual basal MET channel activity in the SO3 neuromast hair cells of *lhfpl5b*^{vo35} mutants and *lhfpl5a*^{tm290d}; *lhfpl5b*^{vo35} double mutants. FM 4-64 labeled SO3 neuromasts from wild type (**A**), *lhfpl5a*^{tm290d} (**B**), *lhfpl5b*^{vo35} (**C**), and *lhfpl5a*^{tm290d}; *lhfpl5b*^{vo35} (**D**) larvae at 5 dpf. Scale bar = 5 µm, applies to all panels.

811

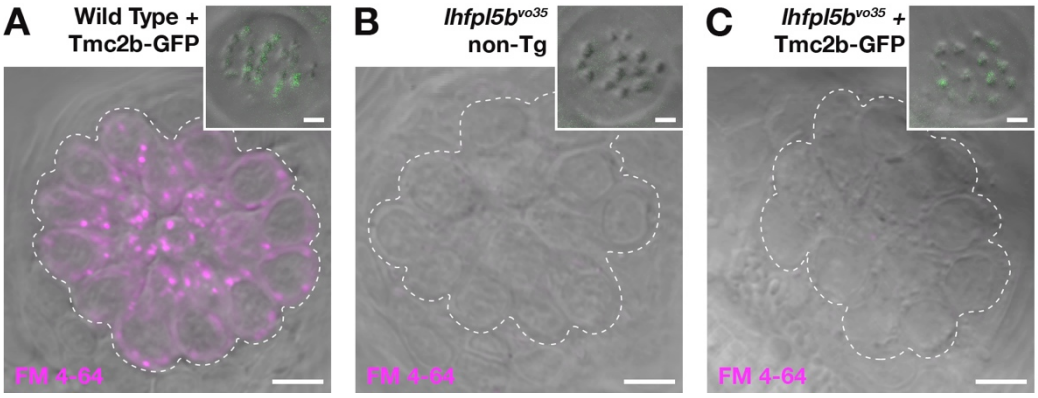

812

813

814 **Supplemental Figure 2.** Bundle-localized Tmc2b-GFP does not restore basal MET channel activity
815 to neuromast hair cells of *lhfpl5b*^{vo35} mutants. (**A-C**) Representative images of neuromasts labeled with
816 FM 4-64 from wild type Tmc2b-GFP *vo28Tg* (**A**), non-transgenic *lhfpl5b*^{vo35} (**B**), and *vo28Tg*;
817 *lhfpl5b*^{vo35} (**C**) larvae at 7 dpf. Dashed lines outline the cluster of hair cells in each neuromast. Insets
818 show the neuromast hair bundles from the same neuromast in the main panel. Scale bars = 5 µm in A-
819 C; 2 µm for the bundle insets.

820

821

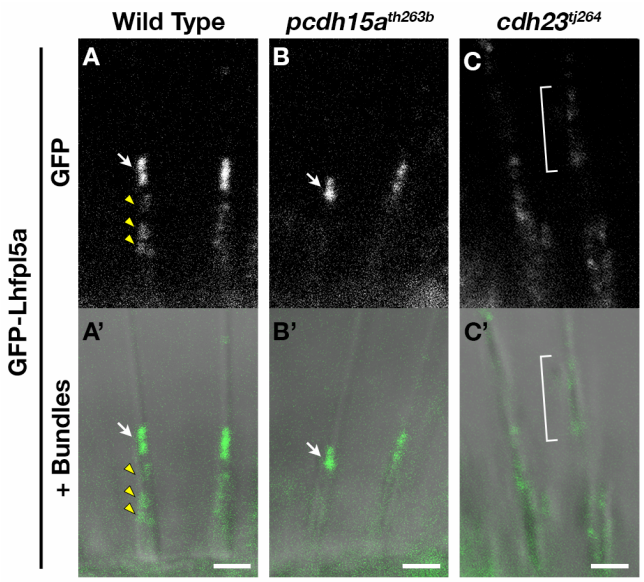

Supplemental Figure 3. Mislocalization of GFP-Lhfpl5a in different mutant alleles of *pcdh15a* and *cdh23* as shown in Figure 6. Representative images of GFP-Lhfpl5a (*vo23Tg*) in the lateral cristae hair bundles of wild type (**A, A'**) and *pcdh15a*^{th263b} (**B, B'**), and *cdh23*^{tj264} (**C, C'**) mutants. The GFP-only channel is shown in panels A - C and overlaid with a light image of the bundles in A' - C'. White arrows indicate GFP signal in the presumptive kinocilial linkages, yellow arrow heads indicate GFP signal in the stereocilia, and brackets indicate GFP signal in the kinocilium. Scale bars = 2 µm in A-C'.